Review

Solid-Phase Optical Sensing Techniques for Sensitive Virus Detection

Elif Seymour , Fulya Ekiz Kanik , Sinem Diken Gur , MONIREH Bakhshpour-Yucel , Ali Araz , Nese Lortlar Unlu , M. Selim Ünlü *

Posted Date: 27 April 2023

doi: 10.20944/preprints202304.1013.v1

Keywords: Solid-phase optical biosensors; virus diagnostics; fluorescence-based sensors; surface plasmon resonance; optical resonators; interferometric biosensors; single virus detection

Review

Solid-Phase Optical Sensing Techniques for Sensitive Virus Detection

Elif Seymour [1,6,†], Fulya Ekiz Kanik [2,†], Sinem Diken-Gür [3], Monireh Bakhshpour-Yucel [2,4], Ali Araz [5], Nese Lortlar Ünlü [6] and M. Selim Ünlü [2,6,*]

[1] Lunenfeld-Tanenbaum Research Institute, Mount Sinai Hospital, Toronto, ON, M4P 1R2, Canada; elif.seymour@gmail.com
[2] Boston University, Dept. of Electrical Engineering, Boston, MA, 02215, USA; fulyaekiz@gmail.com
[3] Hacettepe University, Dept. of Biology, Ankara, Türkiye; sinemmdiken@gmail.com
[4] Bursa Uludag University, Dept. of Chemistry, Bursa, Türkiye; monir.b1985@gmail.com
[5] Dokuz Eylül University, Dept. of Chemistry, Izmir, 35390, Türkiye; aliaraz272@gmail.com
[6] Boston University, Dept. of Biomedical Engineering, Boston, MA, 02215, USA; nese.lortlar@gmail.com
* Correspondence: selim@bu.edu
† These authors contributed equally to this work.

Abstract: Viral infections can endanger public health by causing serious illness, leading to pandemics and burdening healthcare systems. Moreover, in the situation of a global spread, disruptions occur in every aspect of life including business, education, and social life. Fast and accurate diagnosis of viral infections has huge implications for saving people's lives, preventing spread of the diseases, and minimizing social and economic damages. In the last decades, polymerase chain reaction (PCR) based techniques have been frequently used to detect viruses in the clinic. However, in a situation where rapid virus detection is the primary measure in preventing the spread, as in the case of ongoing COVID-19 pandemic, disadvantages of PCR, such as long processing times and requirement of sophisticated laboratory instruments, have been faced. Due to the urgent need for accurate techniques for virus detection, biosensor systems involved in many applications in biological detection are being developed for rapid, real-time, and high-throughput detection of viruses. Among various sensing platforms, optical devices are of great interest due to their advantages such as high sensitivity and direct readout. In the current review, usability of sensing techniques depending on optical phenomena, such as fluorescence-based sensors, surface plasmon resonance (SPR), surface enhanced Raman scattering (SERS), optical resonators and interferometry-based platforms, is discussed for virus diagnostics applications. Then, we focus on an interferometric biosensor developed by our group, single-particle interferometric reflectance imaging sensor (SP-IRIS), which has the capability to visualize single nanoparticles, to demonstrate its application for digital virus detection.

Keywords: solid-phase optical biosensors; virus diagnostics; fluorescence-based sensors; surface plasmon resonance; optical resonators; interferometric biosensors; single virus detection

1. Introduction

Viral infections can pose a serious threat to public health as demonstrated by the ongoing COVID-19 pandemic that started in December 2019, that was caused by a novel coronavirus, SARS-CoV-2, infecting 676 million people and causing 6.8 million deaths worldwide as of March 2023 [1]. Human history witnessed several outbreaks caused by viruses such as the plague [2], cholera [3], flu [4] and HIV [5]. The 1918 Spanish flu pandemic that was caused by H1N1 virus was the deadliest flu pandemic in recorded human history with an estimated 50 million deaths worldwide [6]. Recent COVID-19 pandemic and constant emergence of new outbreaks such as Ebola, Zika, RSV, and monkeypox, highlighted the urgent need for sensitive and high throughput viral diagnostic techniques. It is crucial to detect viral infections in a fast and sensitive fashion for starting appropriate isolation procedures and therapy thus enabling the control of the spread of the viral infection and improving patient care. Laboratory techniques used in the virus diagnostics include virus culture, electron microscopy, enzyme-linked immunosorbent assay (ELISA) for serological analysis, and

polymerase chain reaction (PCR). Virus culture, referred to as 'old gold standard', is performed by growing viruses in cell culture and takes 2-12 days [7]. Long culture time combined with low sensitivity caused replacement of this technique with molecular testing in most of the clinical diagnostic laboratories. Electron microscopy (EM) has been a powerful technique for identification of viruses especially when the causative agent of the viral infection is unknown [8]. Transmission electron microscopy (TEM) can provide high resolution images of viruses and elucidate morphological features such as shape and size. Once family-level classification is done, it becomes possible to determine what molecular assays to use for further identification of the virus species. Despite being crucial for initial identification, due to complicated sample preparation steps and expensive and sophisticated instrumentation, EM is not practical to implement in a workflow that requires high-throughput testing when the demand is extremely high as in the COVID-19 pandemic [9]. Serological detection by ELISA is based on detection of antibodies produced by the immune system as a result of the viral infection. This approach is not very useful for detection of acute infection since the antibodies generated remain in the blood for prolonged periods of time. Polymerase Chain Reaction (PCR) is the current gold standard for virus diagnostics in clinical settings and is based on detection of virus-specific nucleic acid sequences using a mixture of reagents (primers, DNA polymerase, dNTPs, Mg etc.) and the nucleic acid extracted from the patient sample. Although PCR is an extremely sensitive detection technique, it requires highly automated equipment for nucleic acid extraction and expensive thermocyclers for real-time detection of amplified sequences as well as skilled users to operate these instruments. As revealed during the peak times of the COVID-19 pandemic, reagent and trained personnel shortages, insufficient equipment for nucleic acid extraction and RT-PCR, led to long turnover times, overwhelming the laboratories and delaying the results. Due to these limitations associated with laboratory-based diagnostics and an increase in the demand for rapid detection of pathogens for public health and biodefense concerns, there has been considerable effort towards developing alternative detection techniques that can meet high-throughput requirements in easy-to-use and portable platforms. An ideal viral diagnostic platform should be highly sensitive, fast, high-throughput, easy-to-use and also require minimal sample processing and temperature-sensitive reagents. Since the first biosensor which was developed in 1956 by Leland C. Clark for detecting oxygen, there has been tremendous advancements in the biosensor field [10]. Biosensors hold great potential for being used as virus diagnostic tools at the point-of-care owing to the advantages they offer such as simple workflows, cost-effectiveness, portability, and rapid answers. Moreover, integration of the microarray and microfluidics technologies into biosensors enabled multiplexed detection and use of less sample and reagent volumes compared to the laboratory techniques such as ELISA. Biosensors consist of a biological sensing element for specific analyte binding and a transducer system to convert the binding events to a measurable signal. Biosensors can use electrical, optical, or mechanical transduction mechanisms to convert the changes induced by the biological interactions on the sensor to an observable output, which then can be correlated to the biological binding interactions.

In this review, we will focus on optical sensors for virus diagnostics applications. Optical sensors have advantages compared to other transduction mechanisms due to direct detection capability and minimal dependence on the environmental conditions [11]. For viral diagnostic applications, an optical biosensor can be used to determine the presence of an infection by detecting viral antigens, whole viruses, viral nucleic acids or individual's antibody response in biological samples. In solid-phase biosensors, capture agents against one of these analytes are immobilized on the sensor surface. The solid-phase optical biosensors that will be covered in this review include fluorescence-based optical sensors, colorimetric biosensors, surface plasmon resonance (SPR), surface-enhanced Raman scattering (SERS), optical resonators, and interferometry-based platforms including single-particle interferometric reflectance imaging sensor (SP-IRIS), a label-free biosensor developed by our group.

2. Solid-phase Optical Sensors and Their Applications in Virus Detection

Optical biosensors focus on measurement of the optical signals as the changes in the optical properties and characteristics on the transducer surface in the case of an interaction of the

Preprints (www.preprints.org) | NOT PEER-REVIEWED | Posted: 27 April 2023 doi:10.20944/preprints202304.1013.v1

immobilized biorecognition element with the measured substance [12–14]. Figure 1 shows a general illustration of an optical biosensor. In general, the optical biosensor typically consists of an optical source, a transduction platform and an optical detector. The optical biosensor can have different types of biological materials such as antibodies, aptamers, peptides, nucleic acids, peptide nucleic acids, proteins, enzymes, whole cells as the biosensing element on the transducer surface which are designed to bind with the target substance specifically [15–19]. The optical transducer is integrated with the biosensing element closely, and the optical biosensors are classified based on their transducers. The optical biosensors can also be classified based on the dependence on a label for signal generation as label-based and label-free. In label-free biosensors, the signal produced by the interaction of the target and the biorecognition element is measured directly. In contrast, in the label-based biosensors, the detected signal originates from the complex formed by a label, such as a fluorophore or a chromophore, and the target on the transducer. In this section, we discuss a number of selected surface-based optical biosensor technologies for detection of viruses with an emphasis on their fabrication approaches and application areas.

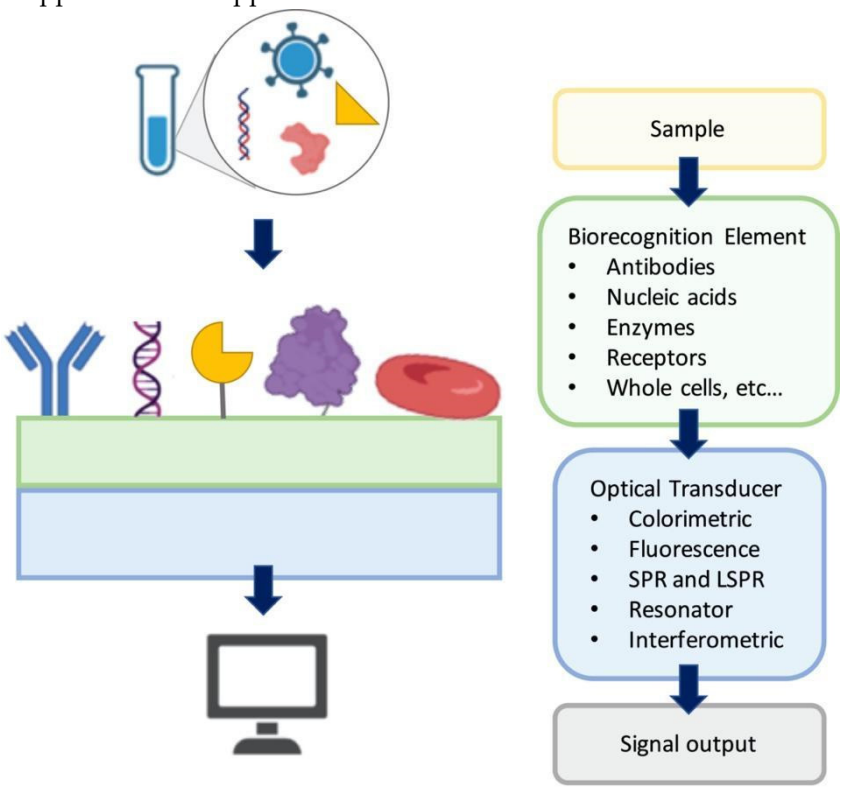

Figure 1. A general illustration of optical biosensors.

2.1. Fluorescence-based optical sensors for virus detection

Fluorescence-based optical biosensors employ the fluorescent labels to produce the optical signal which rely on detecting the fluorescence signal as a result of analyte capture on the transducer [12,20,21]. They are widely used in assay development owing to numerous commercially available fluorescent labels, uncomplicated labeling methods, multicolor fluorophores for multiplexed assays, fast response times with localized fluorescence signal, high temporal resolution and sufficient detection sensitivity [22]. These advantages of fluorescence detection qualify as desirable in the detection of viruses and biological molecules [23–26]. However, certain limitations such as fluorophore blinking, photobleaching and insufficient detection limits for some target molecules make fluorescence-based optical biosensors less applicable in certain applications, for instance in detection of low abundance nucleic acids [27]. Moreover, nonspecific binding of the fluorescent labels to the other components in the sample media remains as an issue in fluorescence detection systems [28]. Besides, irreversible photobleaching of the fluorescent label restrains observation time, hence,

Preprints (www.preprints.org) | NOT PEER-REVIEWED | Posted: 27 April 2023 doi:10.20944/preprints202304.1013.v1

affects the reliability of the test [29]. Here, we present a number of fluorescence-based biosensor applications for virus detection.

A multiplex imaging array was developed for rapid and low-cost diagnosis of trace avian influenza virus (AIV) using DNA biomarkers by Jiang et al. (Figure 2) [30]. They detected three subtypes of AIV DNA biomarkers (H1N1, H7N9 and H5N1) simultaneously using fluorescence imaging and gray-level analysis. They utilized a smartphone for imaging output and completed detection in 20 min. They employed catalytic hairpin assembly (CHA) amplification reactions and utilized thioflavin T, a specific G-quadruplex fluorescence probe for labeling. They reached detection limits of 136 pM, 141 pM and 129 pM for H1N1, H7N9 and H5N1, respectively. Also, the array sensors exhibited excellent anti-interference among the different subtypes and good mismatch discrimination in real sample application. Such a system can easily be applied for early detection of disease diagnostics in low-resource settings.

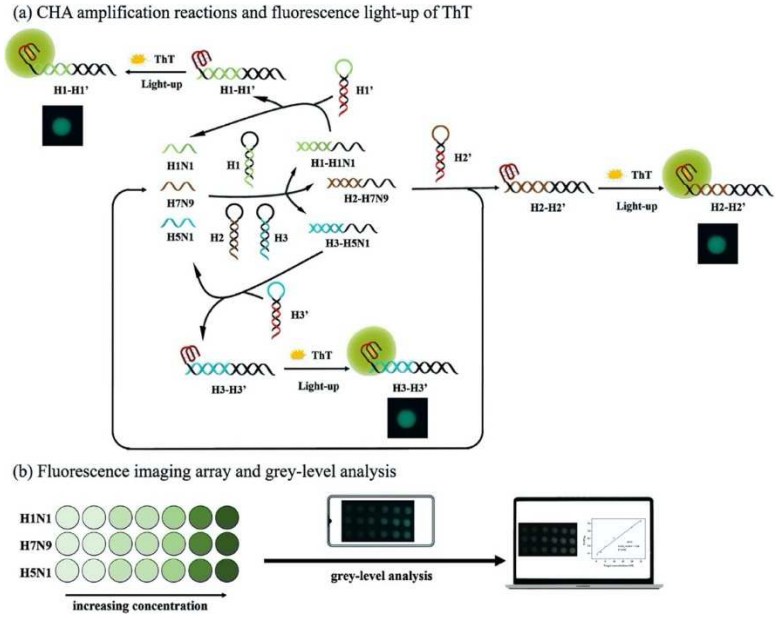

Figure 2. Multiplex imaging array design for rapid diagnosis of trace avian influenza virus (AIV) using DNA biomarkers based on (a) CHA amplification reactions and (b) fluorescence imaging array and gray-level analysis. Reproduced with permission from [30].

Another rapid viral detection and identification study was performed by Hepp et al. for detecting influenza virus, avian infectious bronchitis virus and SARS-CoV-2 specifically and quantitatively in approximately 20 min (Figure 3) [31]. They used fluorescence in situ hybridization (FISH) protocol, specifically rapid viral FISH protocol (rvFISH), where they used fluorescence microscopy to spatially detect and quantify DNA and RNA inside fixed cells and tissues using complimentary and fluorescently labeled oligos. They were able to detect influenza particles and infectious bronchitis virus (IBV), an avian coronavirus, down to a concentration of 10^5 PFU/ mL and 10^2 PFU/ mL, respectively, in a 20-min assay.

Preprints (www.preprints.org) | NOT PEER-REVIEWED | Posted: 27 April 2023 doi:10.20944/preprints202304.1013.v1

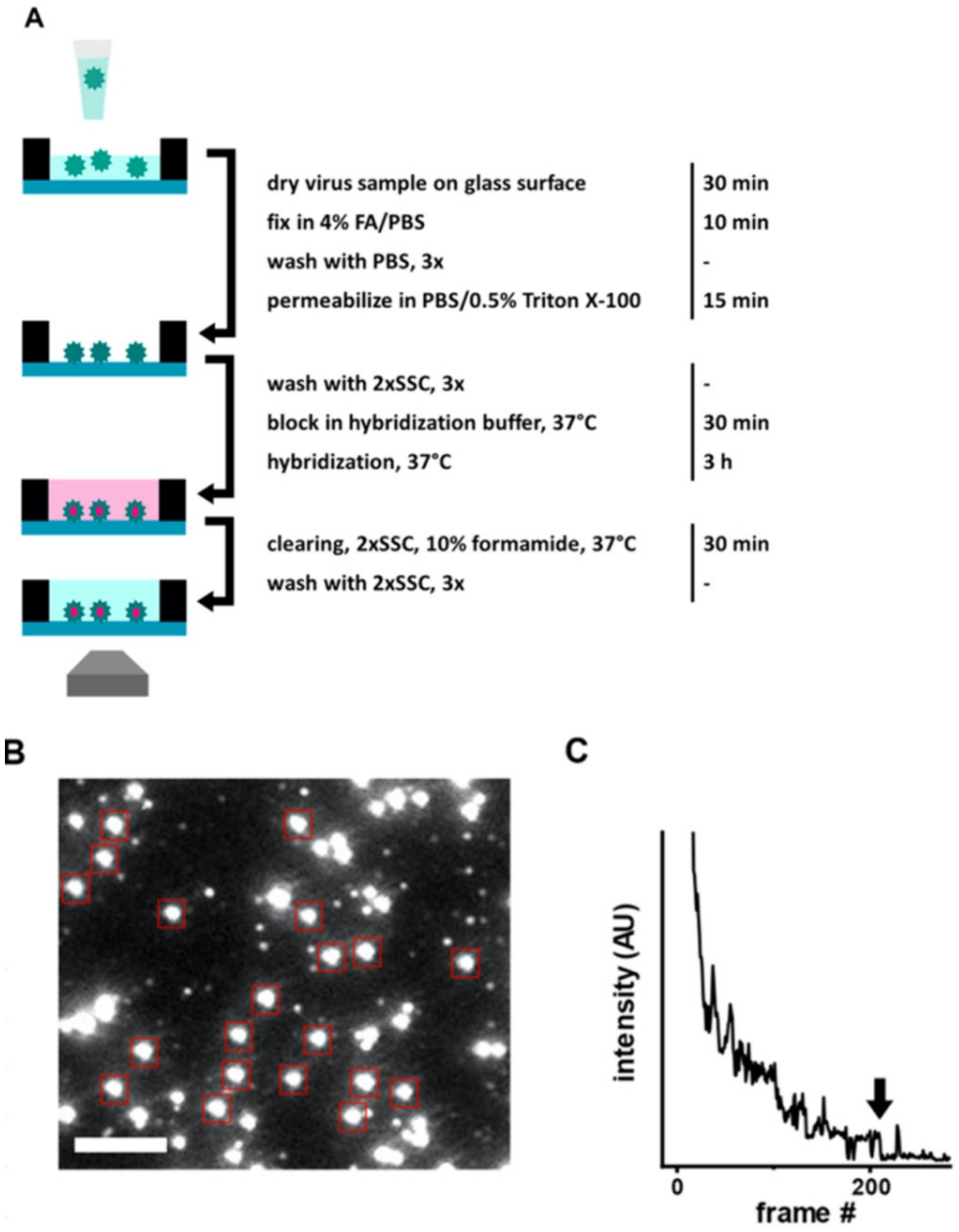

Figure 3. (A) Illustration of FISH -based virus detection. (B) Image of an array after staining with 48 fluorescent hybridization probes for influenza A/WSN/33 virus particles (10^6 PFU/mL). Red boxes point diffraction-limited, isolated particles which were analyzed with stepwise photobleaching. Scale bar 3 μm. Reproduced with permission from [31].

Shiaelis et al. present a methodology for virus detection and identification that uses a convolutional neural network to distinguish between microscopy images of fluorescently labeled intact different viral particles (Figure 4) [32]. They used single-particle fluorescence microscopy and deep learning. The assay successfully performed labeling, imaging, and virus identification in less than 5 min and did not require any lysis, purification, or amplification steps. They carried out two clinical tests of the method using 155 patient samples in total, which provided high overall sample accuracies of 98.0% and 97.1%.

Preprints (www.preprints.org) | NOT PEER-REVIEWED | Posted: 27 April 2023 doi:10.20944/preprints202304.1013.v1

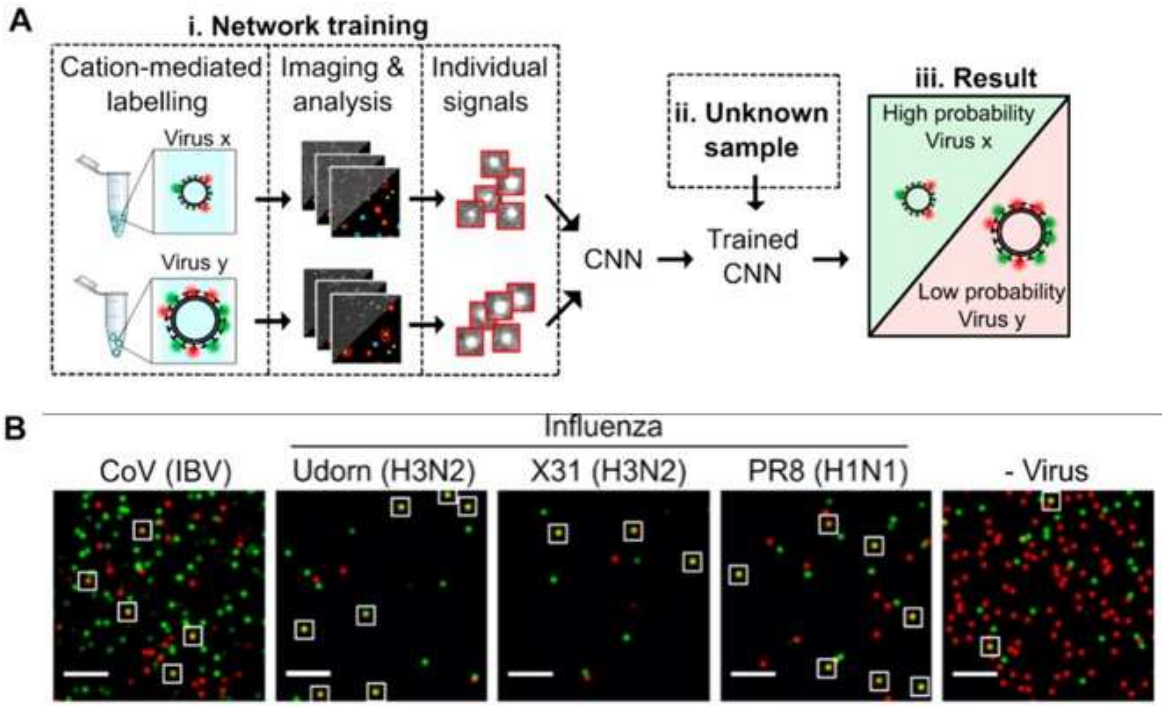

Figure 4. (A) Illustration of the steps how the viruses were labeled and imaged to identify and classify different viruses using trained CNN. (B) Sample field of views for CoV (IBV), two strains of H3N2 influenza (A/Udorn/72 (Udorn) and A/Aichi/68 (X31)), an H1N1 influenza strain (A/PR8/8/34 (PR8)) detection and a negative control. White boxes were used to point out merged red and green localizations as an example of colocalization. Scale bar, 10 μm. Reproduced with permission from [32].

Moreover, Yeo et al. have demonstrated a field-level fluorescent lateral flow immunoassay which was combined with a smartphone-based fluorescent diagnostic device with an efficient reflective light collection module for the detection of avian influenza (AI) (H5N1, H5N3, H7N1, and H9N2) (Figure 5) [33]. Fluorescence light efficiency was improved with the use of latex beads along with the coumarin-derived dendrimer-based fluorescent as anti-influenza nanoparticles. lowest detectable virus titers were found as 6.25×10^3 PFU/mL for H5N3, 5.34×10^2 PFU/mL for H7N1 and 5.23×10^1 PFU/mL for H9N2 in throat swab samples. In addition, clinical validation of smartphone-based diagnostic device with H5N1-infected patient samples was completed within 15 min with sensitivity of 96.55% (28/29) [95% confidence interval (CI): 82.24 to 99.91] and a specificity of 98.55% (68/69) (95% CI: 92.19 to 99.96) ($P < 0.0001$).

Preprints (www.preprints.org) | NOT PEER-REVIEWED | Posted: 27 April 2023 doi:10.20944/preprints202304.1013.v1

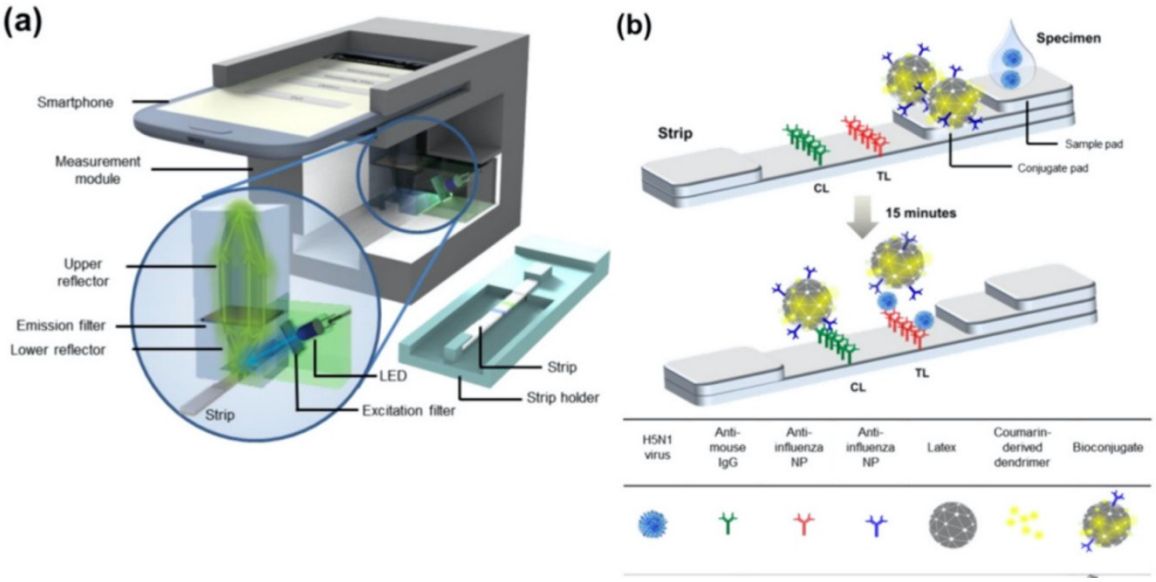

Figure 5. (a) Illustration of the fluorescence detector design using a smartphone and fluorescent lateral flow strip. (b) Illustration of the fluorescence lateral strip for influenza A and the components for lateral flow strip design. A nitrocellulose membrane as the base was decorated with anti-influenza A nucleocapsid (NP) antibody on the test line (TL) and anti-mouse IgG on the control line (CL). Bioconjugate-AI virus complex is captured by the anti-influenza NP on the TL. On the other hand, the unreacted bioconjugates are captured by the anti-mouse IgG on the CL. The fluorescence intensity is measured using the smartphone-integrated diagnostic device. Reproduced with permission from [33].

2.2. Colorimetric biosensors for virus detection

Colorimetry-based biosensors allows visual detection via a change in color by naked eye or simple, low-cost portable optical detectors. These features make them proper candidates to fabricate point-of-care devices that can be used for rapid and cost-effective virus detection [34]. They employ a simple platform with quick response and fair sensitivity, selectivity [35]. In colorimetry-based solid-phase biosensors, on the sensor surface, which is usually a simple test strip, when the sample solution is introduced, a ligand-target complex is formed on the solid support. This complex results in a shift in color which can be easily observed for quantitative measurements. With the recent advancements in nanotechnology, progress has been made in improving the sensitivity of colorimetric detection systems by using various functional nanomaterials such as metal and metal oxide NPs, quantum dots, graphene and derivatives [36]. In the NP-based approach, colloidal NPs that change color during aggregation or dispersion are conjugated with the biosensing element. Plasmonic-based colorimetric biosensors benefit from the localized surface plasmon resonance (LSPR) extinction coefficient in the visible range of noble metal NPs such as gold NPs (AuNPs). Binding event between the analyte and the AuNPs conjugated bioreceptor cause visible color change to detect viruses [37]. NP-based colorimetric sensors can be used in a wide range of virus sensing applications. Parker and coworkers designed an immunoassay-based sensing technique which detected hepatitis E virus (HEV) real-time using Ag-decorated AuNPs. While anti-HEV IgG antibodies were used as conjugate to AuNPs in the inner part, in situ silver deposition was achieved on the outer part as a signal amplification strategy. The virus particles were entrapped by the utilized nanocomposites whereas 3,3′,5,5′-tetramethylbenzidine (TMB) and H_2O_2 were added to decompose back Ag-shell to Ag^+. After addition of TMB- H_2O_2, based on the obvious color change, the concentration of HEV was quantified and real-time monitoring of HEV in real sample was realized [38].

Paper-based lateral flow immunoassays (LFIAs) as point-of-care devices are widely used for early disease diagnostics. Despite its widespread use, it is often limited due to insufficient sensitivity for required sample sizes and short time frames of testing. Loynachan et al., designed a highly

Preprints (www.preprints.org) | NOT PEER-REVIEWED | Posted: 27 April 2023 doi:10.20944/preprints202304.1013.v1

sensitive and serum-stable paper-based, nanoparticle catalyst-labeled LFIA for the detection of a viral capsid protein, p24, one of the earliest and most conserved biomarkers of HIV. They used porous platinum core-shell nanocatalysts (PtNCs), and then explored the application of antibody-functionalized PtNCs with high affinity and specificity modified nanobodies toward p24 and established the key larger nanoparticle size regimes needed for efficient amplification and performance in LFIA [39]. In another study, Wang et al. designed a rapid diagnostic platform integrated with a low-cost reader and a multicolor and a multicolor 4-plex immunoassay to detect and distinguish between dengue virus (DENV) and chikungunya virus (CHIKV) IgM/IgG [40]. The developed platform employs unique color-mixing encoding and quantitative readout strategy while using an optical reader designed to minimize variations in color detection. This provides a consistent multiplexed detection of dengue and chikungunya IgM/IgG antibodies in human clinical samples within 30 min (Figure 6). The multiplex assay requires low sample volumes and has ability to test four samples simultaneously, which makes the rapid diagnostic platform a great candidate to be used in resource-limited settings.

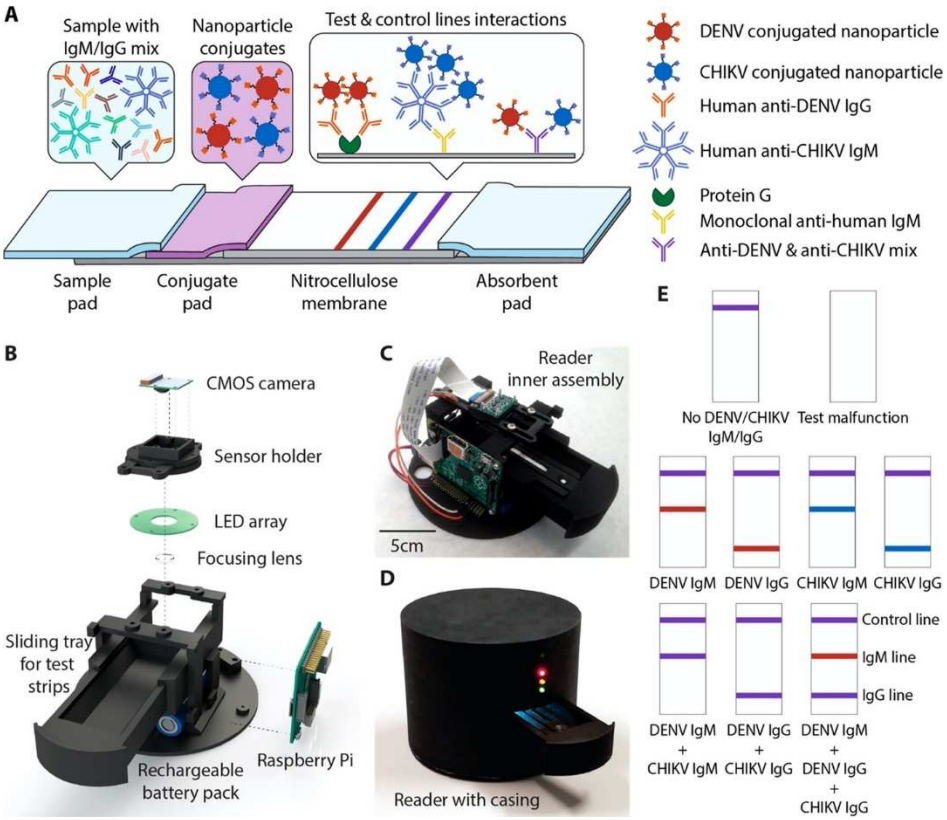

Figure 6. A) A 4-plex colorimetric lateral flow test strip and an optical readout device. Red and blue nanoparticle conjugates in the conjugate pad bind to DENV and CHIKV antibodies in the sample, respectively. Nanoparticle-IgG complexes are captured by the first test line (red), and nanoparticle-IgM complexes are captured by the second test line (blue), causing a color change. When both DENV and CHIKV antibodies of the same isotype are present, a mixture of red and blue appears at the test line. Unbound nanoparticle conjugates are captured at the control line (purple). (B) Parts of the optical reader. (C) Inner view of the optical reader. (D) Fully assembled version of optical reader with lightproof casing. (E) Examples showing the color development on the test strip for various cases. Reproduced with permission from [40].

 doi:10.20944/preprints202304.1013.v1

2.3. Virus detection with Surface Plasmon Resonance and Localized Surface Plasmon Resonance

Surface plasmon resonance (SPR) is defined as an electromagnetic (EM) phenomenon depending on collective resonant oscillations of free electrons and incoming protons passing through metal-dielectric interface. The working principles of SPR-based optical sensors depend on the detection of changes in refractive index that arise on the dielectric surface near the metal layer [41,42]. The properties of this metal layer strongly influence the SPR response that is generated according to refractive index change. The metals which have conduction band electrons, such as gold, silver, aluminum, and copper, show capability for resonating at an appropriate wavelength with the incident light. Gold is the most preferred metal film due to its chemical stability and sensitivity for sensing applications [43]. A typical SPR experiment consists of three main components (i) immobilized recognition element, (ii) the prism of light, (iii) analyte [44]. The recognition molecule is immobilized onto the gold surface of the sensor chip. After surface functionalization, a sample solution containing the analyte is passed across the chip surface. Incident light passing through the prism excites the electrons of the metal film to form surface plasmon. As the incident light reaches the medium at various angles, the photons are absorbed by the plasmon wave at a specific angle, as critical angle, which is affected by the refractive index of the medium. When an analyte binds to the immobilized recognition element, due to the mass accumulation on the immobilized layer, the refractive index of the medium near the chip surface changes, which shifts the critical angle for the immobilized molecule [45–47]. Thus, any physical changes that cause refractive index change can be monitored without labeling in real time. SPR-based sensing techniques emerge with high potential in diagnostics with their magnificent properties referred above, to accomplish rapid and point of care (POC) detection of viruses. Antibodies against viral antigens and surface proteins are used as bio-receptors to capture viral proteins and intact viruses while preparing sensor chip surfaces. Additionally, artificial recognition sites obtained by molecular imprinting or laboratory made capturing molecules such as DNA and RNA aptamers are used to capture several viruses [48]. SPR sensing technology, which is highly accurate in detecting biomolecular interactions, also offers various advantages of label-free monitoring, rapid and sensitive outcome, and ability to miniaturize for on-site monitoring [49]. However, to succeed in early diagnosis of viruses using SPR method, further enhancements in the selectivity and sensitivity are still required [48]. Here, different SPR-based techniques that can detect viruses are discussed.

Chang et al. developed an intensity-modulated surface plasmon resonance (IM-SPR) biosensor integrated with a lately generated monoclonal antibody which enables rapid and sensitive detection of H7N9 virus due to the avian influenza A H7N9 virus in China [50]. The novel antibody displays important specificity in the H7N9 virus detection. They experimentally reported a detection limit of 144 copies/mL using the proposed approach for the H7N9 virus, which is a 20-fold increase in sensitivity compared with homemade target-captured ELISA. They reported less than 10 min assay time. 10 μg/mL of the captured antibody H7-mAb was covalently immobilized to the reaction spot of the SPR chip through mixed self-assembled monolayers of 11-mercaptoundecanoic acid and 6-Mercapto-1-hexanol (1:9) via the amine coupling protocol (Figure 7). The results demonstrated that the simple SPR-based technology was successfully used in sensitive H7N9 virus detection. They reported that the proposed SPR system can be used in implementations of other emerging virus detection platforms.

As effective and simple methods are needed for virus detection, Yoo et al. designed a reusable magnetic SPR sensor chip for H1N1 influenza virus detection in a conventional SPR sensor. They used ferromagnetic patterns on an SPR sensor chip to prepare a layer of magnetic particles, and a solid substrate for SPR sensing [51]. They demonstrated the system platform which enables repetitive use by removing magnetic particles using external magnetic fields at the end of an experiment without the need for antibody-modifying processes which would be a substantial step toward the future application of virus sensor systems. Figure 8 shows the schematic of the virus detection by antibodies conjugated to magnetic beads on the substrate. Figures 8A,B depict the ferromagnetic nickel patterns and trapping of magnetic particles on the SPR chips, and Figure 8C schematizes the antibody immobilization on magnetic particles using EDC-NHS coupling. Figures 8D,E show the

Preprints (www.preprints.org) | NOT PEER-REVIEWED | Posted: 27 April 2023 doi:10.20944/preprints202304.1013.v1

detection of target molecules, and then removal of the magnetic particles by an external magnetic field, respectively. The ferromagnetic patterns on the sensor chip surface are deflected by the strong external fields so that the large aggregation of magnetic particles on the sensor surface was reduced. This study showed the use of a single reusable SPR chip for the detection of nucleoprotein of H1N1 influenza virus without a drastic signal degradation. The cost of the SPR chip was significantly reduced by reusing the SPR repeatedly.

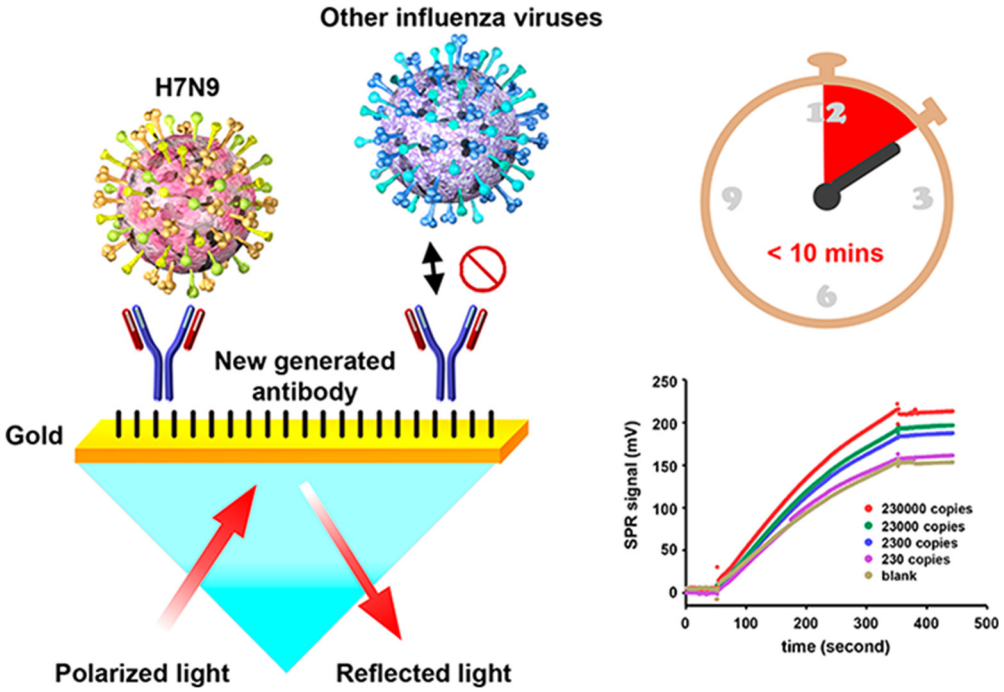

Figure 7. The schematic immobilization of antibody H7-mAb to the reaction spot of the SPR chip. Reproduced with permission from [50].

Receptor-analyte interaction occurring on the surface of plasmonic biosensors is also monitored by localized surface plasmon resonance (LSPR). Unlike SPR, LSPR is formed by a light wave absorbed within conductive nano-plasmonic materials which are smaller than the wavelength of incident light [52]. Owing to the enhanced signal amplification provided with the use of nanomaterials which have important optic, electrical and magnetic features, a low limit of detection can be obtained. While incident light interacts with the metallic nanoparticles (NPs) of the surface, strong localized EM field generated around these nanostructures enables a strong peak in the course of the absorption spectrum collection at resonance [53]. The height of LSPR peak and the corresponding wavelength are affected by not only the sensing medium but also the material type, size, and the shape of the plasmonic NPs. The utilization of the nanoparticles for the decoration of chip surface also provides large surface area to immobilize a high number of bioreceptor molecules, which increases the sensitivity and specificity of the sensing technique. Several metallic nanostructures such as nanospheres, nanofibers, nanorods, nanoshells and nanowires can be used to fabricate sensing surfaces. The dimensions and the shape of these nanostructures directly affect the plasmonic properties (scattering and absorption ratio, resonance wavelength) of them [54]. Two main drawbacks of SPR are escaped with LSPR: firstly, temperature sensitivity is not an issue for LSPR since the method depends on a simple absorbance measurement, secondly, less time is required for the whole binding event due to the faster spread of the analyte to the increased surface area of NPs than metallic film [55,56]. On the other hand, the response produced for non-specific binding as well as for the refractive index variations is the major drawback limiting the applicability and effectiveness of the sensor to detect analytes in complex media [57]. In the last decade, a remarkable increase in the number of nanomaterial-based sensing techniques developed for viral diagnosis has been reported.

Preprints (www.preprints.org) | NOT PEER-REVIEWED | Posted: 27 April 2023 doi:10.20944/preprints202304.1013.v1

Kim et al. developed a unique structure that used gold nanoparticles (AuNPs) to develop a highly sensitive method for hepatitis B surface antigen (HBsAg) detection [58]. They designed a single-layered LSPR chip format via antigen-antibody reaction-based detection symmetry using AuNPs. The virus was sandwiched between two different sizes of AuNP on an AuNP-laden substrate. In their study, two AuNPs in close proximity repulse each other in a plasmon resonance state in the presence of the virus, resulting in a stronger peak shift effect than that in the non-sandwich state. The concentration of HBsAg was reported at 10 pg/mL. They fabricated a modified detection format to further improve the detection limit by fixing a secondary antibody to the AuNP monolayer, which detected a 100 times sensitive detection limit. They showed highly sensitive detection of HBsAg, 100 fg/mL within 10–15 min, using a novel-designed sandwich immunoassay LSPR chip. A diagrammatic of the LSPR biosensor chip is shown in Figure 9. They showed that implementation-based systems have been affected by particle size in using the LSPR.

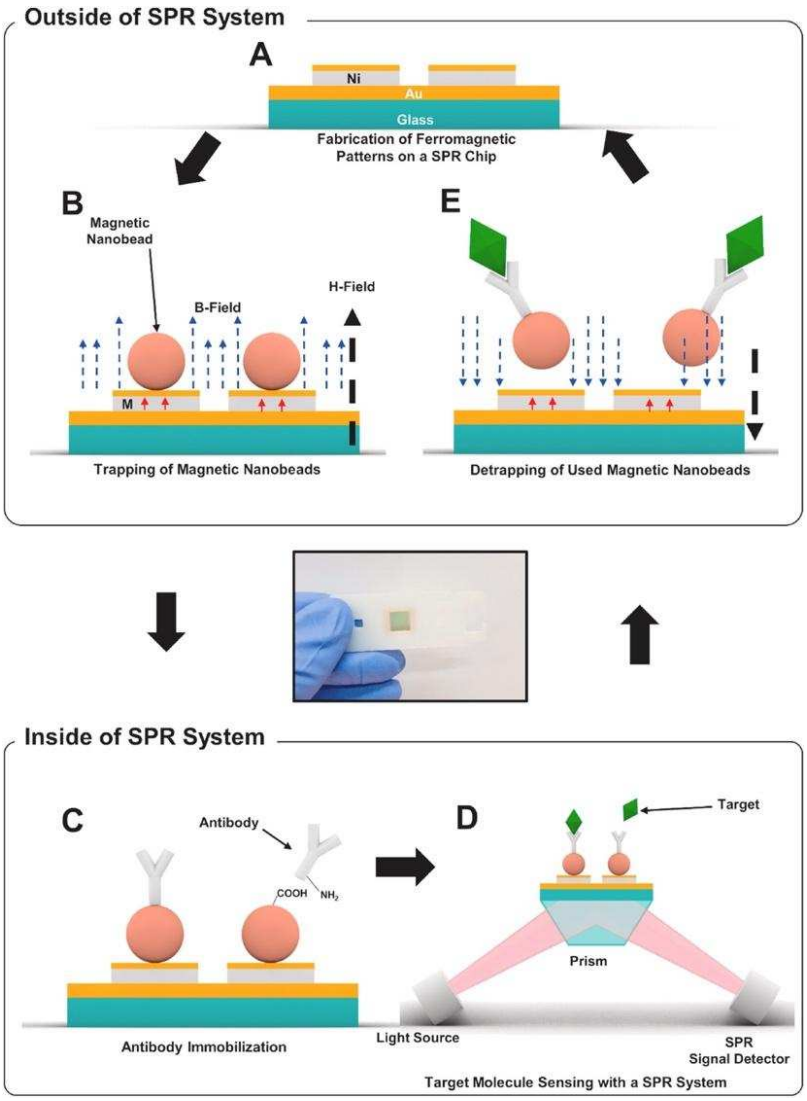

Figure 8. Schematic diagram of reusable SPR biosensor chip, A. ferromagnetic nickel patterns SPR chip, B. Trapping of magnetic particles on the SPR chip through an external magnetic field, C. Immobilization of antibodies on magnetic particles using EDC-NHS coupling in a conventional SPR system, D. Detection process of target molecules, E. Removal of magnetic particles by an external magnetic field in an opposite direction to that for trapping. Reproduced with permission from [51].

Preprints (www.preprints.org) | NOT PEER-REVIEWED | Posted: 27 April 2023 doi:10.20944/preprints202304.1013.v1

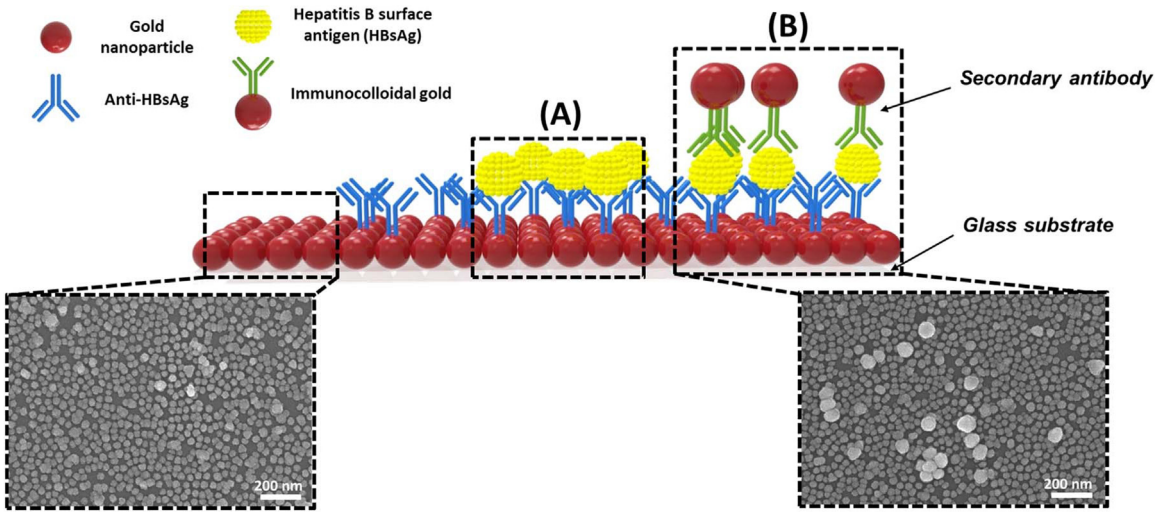

Figure 9. Diagrammatic of LSPR biosensor chip working. AuNPs were arrayed on the glass substrate. (A) Single assay LSPR sensing chip format; (B) modified hetero assembled AuNPs sandwich immunoassay LSPR chip format using immune colloidal AuNPs. Reproduced with permission from [58].

Kim et al. developed a gold nanorod-enhanced surface sandwich assay for norovirus (NoV) capsid protein detection via a novel pair of aptamers, in conjunction with SPR [59]. They used four different DNA aptamer sequences that were known to be specific for the NoV protein to find the strongest binding constant. The aptamer II sequences were covalently bonded onto a chemically modified thin Au chip surface. For the formation of the surface sandwich complex, the NoV-specific aptamer was attached to the surface of the SPR chip which was modified via 1-Ethyl-3-(3-dimethylaminopropyl)-carbodiimide hydrochloride and N-(hydroxy-sulfosuccinimide) solution. Then, NoV capsid protein and gold nanorod- enhanced aptamer were adsorbed. The authors reported a 50 aM limit of detection value for NoV capsid protein after flowing different concentrations of NoV protein solutions over the aptamer-modified chip. The NoV capsid protein concentrations also were analyzed in human serum samples. The schematization of the aptamer-aptamer sandwich assay strategy and representative SPR sensorgrams are shown in Figure 10.

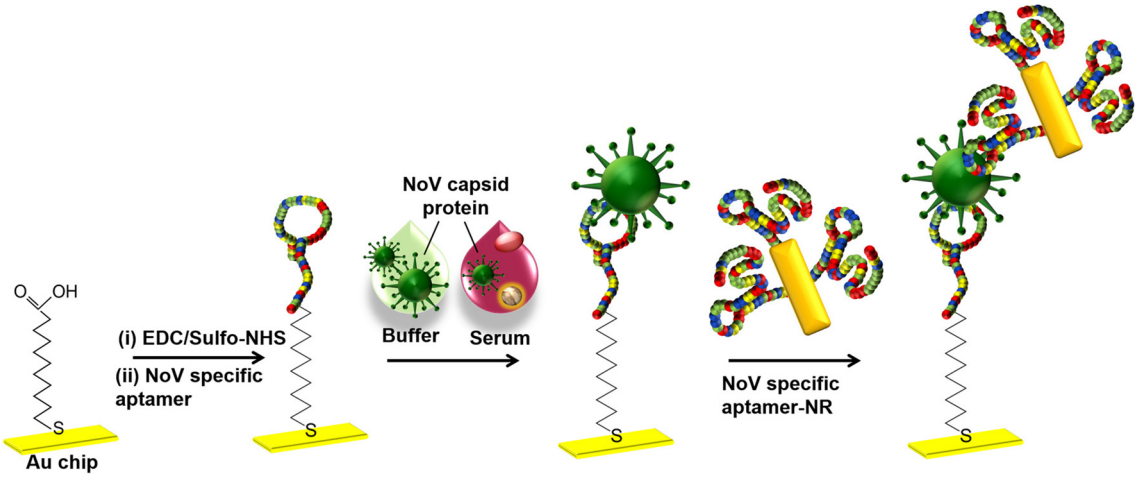

Preprints (www.preprints.org) | NOT PEER-REVIEWED | Posted: 27 April 2023 doi:10.20944/preprints202304.1013.v1

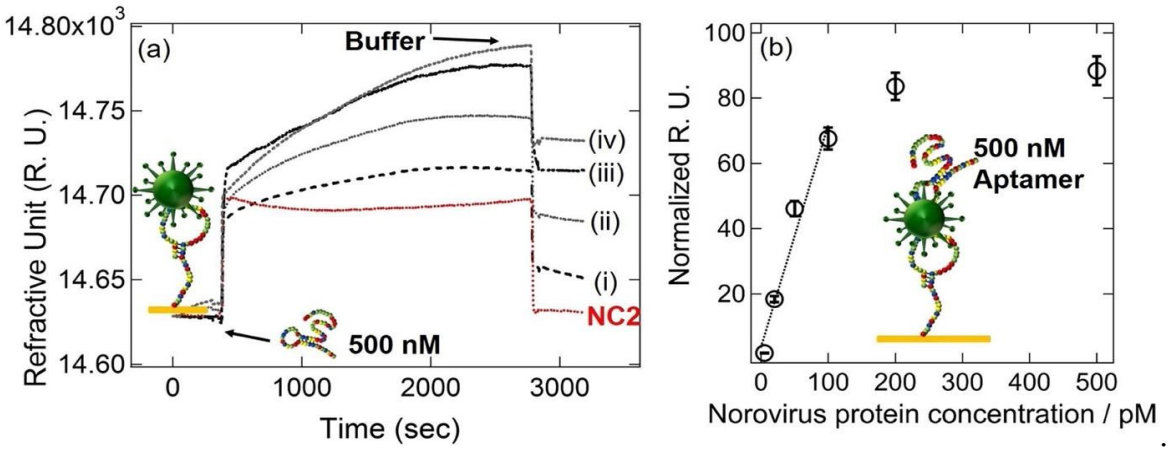

Figure 10. Top: The schematic illustration of the aptamer-aptamer sandwich assay. Bottom: (a) Representative SPR sensorgrams for 20 - 500 pM NoV protein concentrations when 500 nM DNA aptamer I was used, (b) Normalized R. U. responses for the NoV protein sensing. Reproduced with permission from [59].

2.4. Virus detection with Surface-enhanced Raman scattering

Surface-enhanced Raman scattering (SERS)-based sensing platforms have gained attention in the last few decades due to their fascinating advantages: (i) high sensitivity, (ii) capability for multiplex sensing, (iii) applicability as a POC device, (iv) laborless sample preparation [60]. Although Raman spectroscopy is found to be a beneficial tool for analyte determination by providing fingerprints like spectrum for complex samples, its inherently weak signals limit its use for diagnosis. However, in SERS technology, the limitations of the weak Raman signal of Raman-active material are overcome by enhancing the EM field by using metallic nanostructures. The development of high-sensitivity SERS sensors with advanced EM field is carried out by optimizing the design of plasmonic nanostructures [53]. The main advantages of SERS technology are the specific analyte determination ability even at very low concentrations without sample pre-treatment and applicability as a POC device. On the other hand, signal-reducing degradation in the substrate over time due to the requirement for close contact between the analyte and the amplification surface is the main challenge that limits the reproducibility of the SERS signal [61]. SERS-based sensors are dependent on two main methods as direct and indirect. While the direct method relies on the detection of the spectrum of an analyte, in the indirect technique that is constructed as a sandwich-like form SERS signals are getting from the reporter molecule, not the analyte. To differentiate the spectral data of an analyte in the direct technique, main component and linear discriminant analysis need to be performed by comparing the samples of patients and healthy individuals [62]. In the indirect technique, sensitivity of the method reaches at ultra-low concentrations with combining immunoassay strategy to detect analyte. In order to meet the growing need for accurate and rapid virus detection in recent years, multiplex immunoassay-based SERS has become prominent due to the limitations of PCR-based techniques that only require genetic material for testing [63].

Liu et al. used SERS-based lateral flow immunoassay (LFIA) to determine COVID-19 at the point of care [64]. They used Raman molecules to functionalize dual layers of silver shell on SiO_2 core NPs as SERS tags. Anti-human IgM and IgG were immobilized onto the two test lines of the strip to capture the formed SiO_2-Ag-spike (S) protein-anti-SARS-CoV-2 IgM/IgG immunocomplexes. The author used a 785 nm excitation with 10.0 mW laser power. The detection value was 1 ng/mL of the S-protein antibody which was 800 times higher than that of standard gold NPs-based LFIA for template IgM and IgG. A schematic of the dual-layers of Raman reporter molecule 5,5′-dithiobis-2-nitrobenzoic acid (DTNB) modified silica-Ag NPs (SiO_2-Ag) via LFIA is shown in Figure 11. They revealed that the results showed high accuracy and specificity for patients with SARS-CoV-2 infection using the designed method.

Preprints (www.preprints.org) | NOT PEER-REVIEWED | Posted: 27 April 2023 doi:10.20944/preprints202304.1013.v1

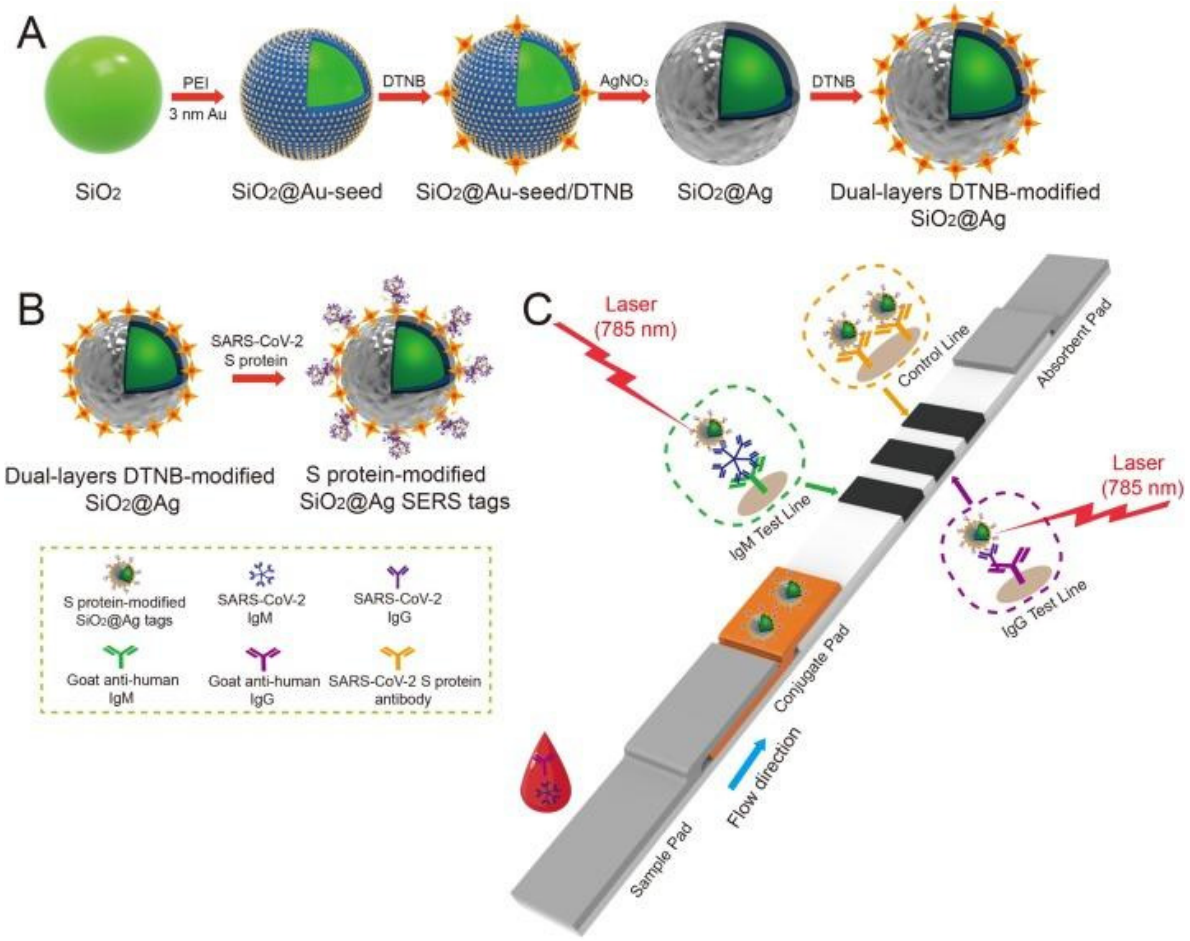

Figure 11. (A) Schematic of the dual-layers DTNB-modified SiO_2-Ag NPs. (B) schematic of the preparation of the SARS-CoV-2 S-protein-modified SiO_2-Ag SERS probes. (C) simultaneous high-sensitivity anti-SARS-CoV-2 IgM/IgG identification using the SERS-LFIA strip's operating concept. Reproduced with permission from [64].

A new SERS detection system was developed by Zhang et al. They used citrate to reduce Ag NPs and added acetonitrile solvent to form a superb hot spot proper for viruses by aggregating Ca^{2+}, and exploring the human adenovirus, SARS-CoV-2 without difference and marker [65]. Then, they showed 100 PFU/test detection limits of viruses within 1 to 2 min when combined with machine learning. Figure 12 shows the experimental process where Ag NPs were modified by bromide ions modified and acetonitrile and Ca ions.

Preprints (www.preprints.org) | NOT PEER-REVIEWED | Posted: 27 April 2023 doi:10.20944/preprints202304.1013.v1

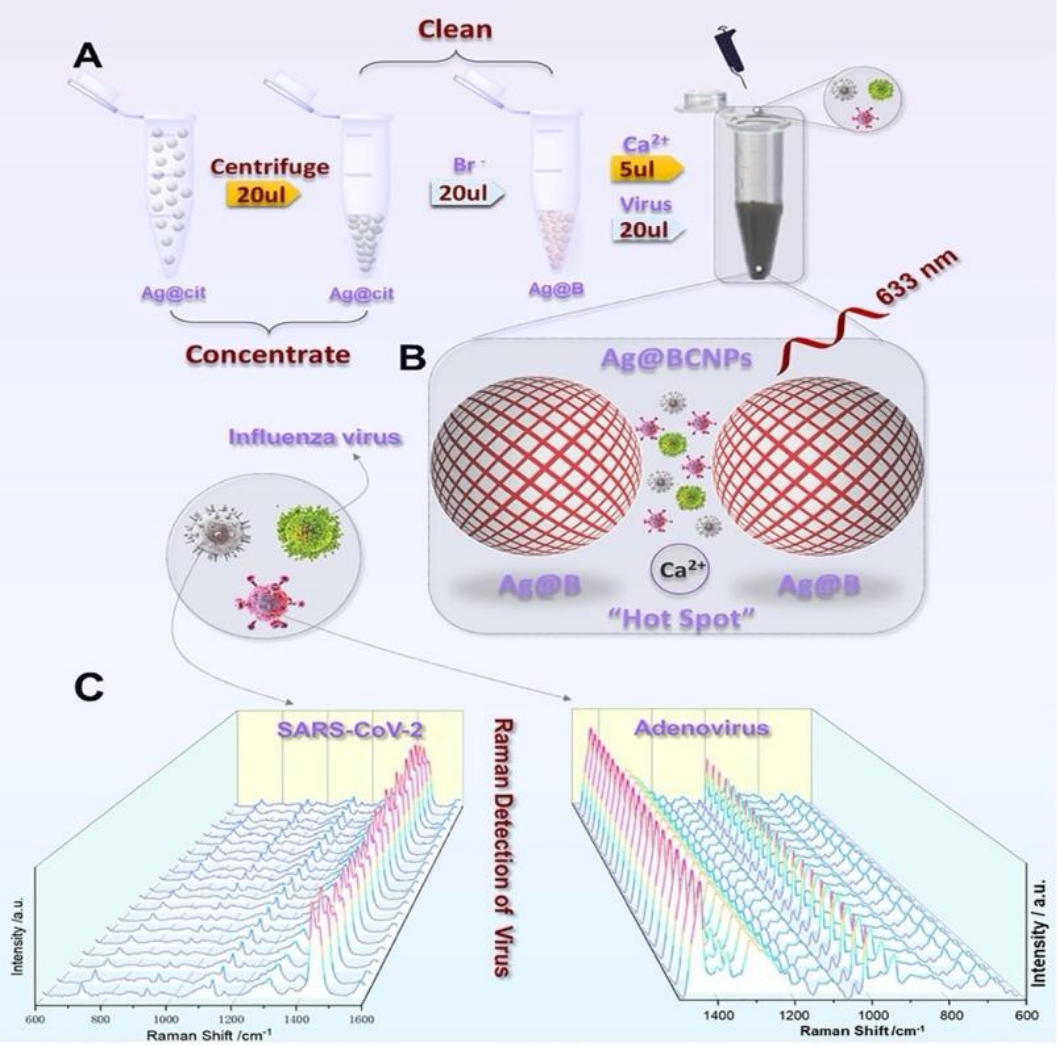

Figure 12. (A) Schematic showing the silver-enhanced substrate preparation and virus detection with the SERS technique. (Ag@cit: Silver NPs formed as a result of reduction of citrate; Ag@B: AgNPs with bromide ion; Ag@BCNPs: Ag@B with acetonitrile and calcium ions added). (B) Schematic illustration of the interaction between the viruses and the "hot spots" produced by the Ag-enhanced substrate. (C) SERS spectra collected from 20 random groups of SARS-CoV-2 (10^4 PFU/test) and HAdV (10^5 copies/test) samples using the Ag@BCNP-based method. Reproduced with permission from [65].

2.5. Optical resonators for virus detection

Optical resonator sensor systems have attracted significant attention in recent years as a powerful tool for detecting a range of biological and chemical analytes with high sensitivity and specificity [66]. These sensors operate by measuring the spectral changes in the resonant frequency of an optical cavity when the analyte is introduced into the cavity. The main principle of an optical resonator sensor is based on the detection of light intensity changes induced by changes in the refractive index of the medium surrounding the resonator. The resonator consists of a thin film layer or a ring resonator that supports resonant modes, which are excited by a laser beam. The resonant modes of the resonator are highly sensitive to changes in the refractive index of the surrounding medium. When a target molecule or virus binds to the resonator surface, it causes a change in the refractive index, which is detected as a shift in the resonant frequency of the resonator [67].

The basic design of an optical resonator sensor consists of a high-quality factor (Q-factor) resonator, such as a microdisk or microring, and a waveguide coupled to the resonator. The resonator acts as a sensitive transducer that is capable of detecting changes in the refractive index of the surrounding environment caused by the analyte binding to the surface of the resonator. The change in the resonant frequency is then measured by monitoring the light transmitted through the waveguide. Fabry-Perot cavities, whispering gallery mode (WGM) cavities, photonic crystal cavities (PC) and plasmonic resonators are some of the most common types of optical resonators [68,69].

For biological particle detection, optical resonators such as microspheres and microtoroids have been used to detect individual virus particles in the size about 100 nm in a label-free format [70,71]. WGM cavities are highly efficient optical resonators, with high Q-factors which allows for the detection of very small changes in the refractive index of the cavity, making them useful for a variety of sensing applications. He et al. developed a WGM microresonator using frequency splitting in a microlaser and showed detection of Influenza A virus on this sensor [72]. Their method relies on measuring the changes in the beat frequency as an ultra-narrow emission line from a WGM microlaser is split into two modes as a result of nanoparticle binding. Before nanoparticles arrive, there is a single laser mode and the laser intensity is constant. The lasing mode splits into two modes when the first nanoparticle binds, leading to a beat note with a frequency that is equal to the difference in frequency between the two modes. Using this approach, they were able to detect sizes down to 15 nm for polystyrene nanoparticles and 10 nm gold nanoparticles as well as Influenza A virus. However, this system was tested with purified nanoparticle and virus solutions and has yet to show multiplexed virus detection from complex biological systems.

As another type of resonator-based sensors, ring resonators have been preferred owing to their unique potential for the ability to be coupled in high-throughput arrays efficiently for multiplexed analysis [73,74]. A rapid detection of an Ebola biomarker with optical microring resonators was performed by Qavi et al. [75]. Soluble glycoprotein (sGP) is the primary product of the glycoprotein (GP) gene of Ebola virus (EBOV), which is a nonstructural secreted GP that is expressed from the unedited RNA transcript. There are several roles sGP appears to play in EBOV pathogenesis, therefore, it is very useful to be utilized as a biomarker in virus detection. In this study, the authors developed a sensor by adapting a silicon photon microring resonator platform to detect EBOV sGP (Figure 13A). The microring resonator sensor detected sGP in under 40 min with a LOD as 1.00 ng/mL in serum which was much lower analytical sensitivity compared to the ELISA tests.

Koo et al reported an isothermal, label-free, one-step RNA amplification and detection system, termed as iROAD, for the diagnosis of respiratory diseases based on silicon microring resonators [76]. Figure 13B shows the chip fabrication and functionalization for the assay. The iROAD assay achieved a one-step viral RNA amplification/detection example to rapid analysis (< 20 min). They have obtained a LOD for the iROAD assay to be 10-times more sensitive than that of real-time reverse transcription-PCR method. The authors tested the iROAD system on 63 human respiratory samples and confirmed its utilization as a more robust operation by using an array of microrings for multiple detection in clinical use.

Optical resonators offer several advantages over traditional optical devices, including high sensitivity, selectivity, and miniaturization. Optical resonators can be designed to have a very high Q-factor, which allows for the efficient coupling between the optical signal and the surrounding environment. However, optical resonators also have some limitations, including sensitivity to temperature and fabrication complexity.

Preprints (www.preprints.org) | NOT PEER-REVIEWED | Posted: 27 April 2023 doi:10.20944/preprints202304.1013.v1

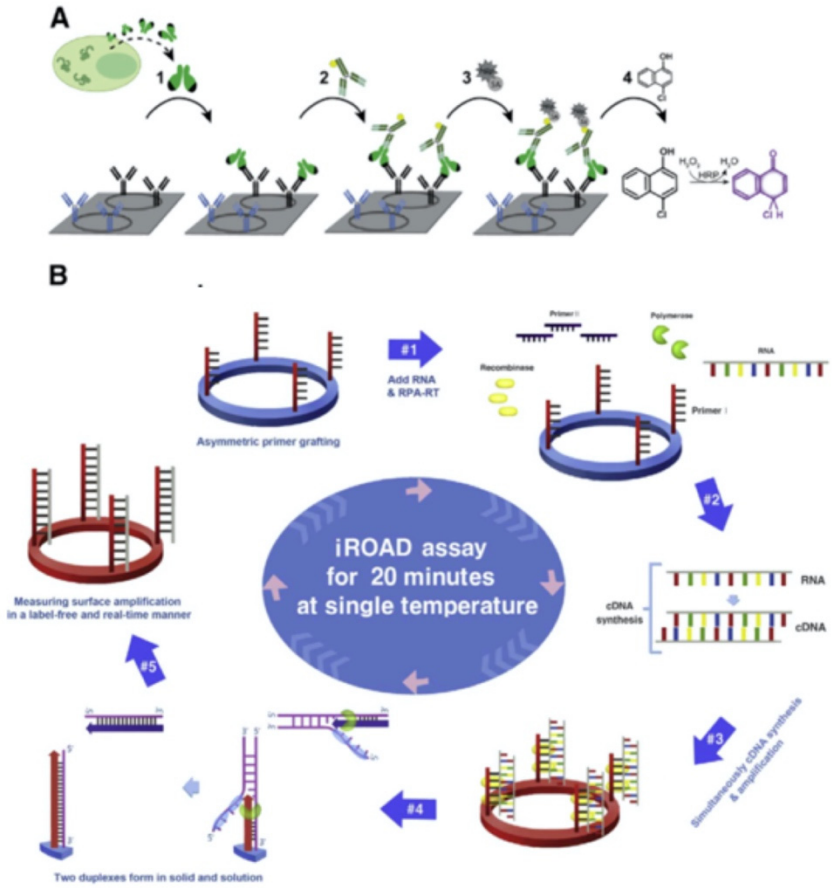

Figure 13. A) Schematic of microring resonator-based detection of sGP (A) Steps of sGP detection using the microring resonator. 1) binding of sGP in the serum sample to the specific antibodies immobilized on the microring surface (black). Blue antibodies represent non-specific antibodies as a negative control, 2) detection of the captured sGP using secondary antibodies which are biotinylated panfiloviral antibodies, 3) addition of streptavidin horseradish peroxidase to detect the sandwich complex, 4) enzymatic reaction. Reproduced with permission from [75]. B) Schematic representation of iROAD assay which involves an isothermal RNA amplification and label-free detection. 1) iROAD chip preparation by forward primer grafting on the sensor, 2) addition of the recombinase polymerase amplification (RPA) reagents, reverse primers, and extracted RNA, 3) cDNA synthesis from the RNA template using RT-RPA, 4) binding of recombinase-primer complexes to cDNA for strand exchange. When the displaced strand makes a D-loop by gp32 (sky blue), primers on the microring surface are extended by polymerase (light green), 5) formation of two duplexes in solid and solution. The amplification is detected by measuring the wavelength shift on the microring resonator for 20 min. Reproduced with permission from [76].

2.6. Interferometry-based sensor platforms

Viruses are difficult to detect using conventional light microscopy which, for the most part, relies on measuring the scattered light by the imaged objects. This is due to their small size (typically 20 – 300 nm in diameter) and low contrast. Light-particle interaction for small-sized particles can be represented by an induced dipole. The strength of an induced dipole is directly proportional to the polarizability of the particle which can be given as

$$\alpha = 4\pi\varepsilon_0 R^3 \frac{\varepsilon_p - \varepsilon_m}{\varepsilon_p + 2\varepsilon_m} \quad (1)$$

where R is the radius of the particle, and ε_p and ε_m are the permittivity of the particle and medium, respectively. The optical techniques that detect scattered light intensity generate a signal proportional to the $|E_s|^2$ which scales with $|\alpha|^2$ thus R^6. Therefore, the scattering signal recorded at the detector

Preprints (www.preprints.org) | NOT PEER-REVIEWED | Posted: 27 April 2023 doi:10.20944/preprints202304.1013.v1

drops below the shot-noise limit for small particles. On the contrary, interferometric imaging utilizes a strong reference beam (E_r) which interacts with the weak scattered fields (E_s) from the particle and modifies the intensity obtained at the detector as

$$I \propto |E_r + E_s|^2 \propto |E_r|^2 + |E_s|^2 + 2|E_r|\,|E_s|\,cos\theta_{rs} \quad (2)$$

where θ_{rs} is the phase angle difference between the reference and scattered fields. As the particles size gets smaller, the scattered field, the second term in the Equation 2, becomes very small compared to the other two terms representing the reference field and the interference signal. Once the reference field is subtracted, the signal recorded at the detector is proportional to the multiplication of the reference and scattered fields, thus proportional to R^3 as opposed to R^6. As a result, interferometric imaging makes it possible to detect smaller particles as well as higher dynamic range of particles sizes. Due to these advantages, interferometry has been utilized for both ensemble-based measurements and single nanoparticle detection in previous studies [77]. One example of ensemble-based measurement technique is biolayer interferometry (BLI), which is a label-free, real-time characterization technique for biomolecular interactions [78]. In this technique, a fiber optic biosensor is used to illuminate the sensor area with white light and the resulting shift in the wavelength of the reflected light is recorded. Although this technique was shown to perform antibody detection with similar sensitivity to ELISA, there are some disadvantages associated with it such as lack of single nanoparticle detection ability and signal jumps as the new solutions are introduced to the well [79]. Interferometry-based nanoparticle imaging techniques have also been developed for single virus detection [80,81]. However, these techniques use cost-inefficient lasers as the light source and can be time consuming due to small measurement area that is on the order of nanometers.

Interferometric reflectance imaging sensor (IRIS), developed by Ozkumur et al., is a label-free biosensor that can probe bimolecular interactions on a silicon/silicon dioxide (Si/SiO_2) substrate in a multiplexed microarray format [82,83]. Detection mechanism of IRIS depends on obtaining the interference signature of the reflected light from Si/SiO_2 substrate and measuring the optical thickness of the top layer (Figure 14). The substrate is a silicon chip with a thermally grown oxide layer which is spotted with capture probes that are specific for the target molecule. Binding of target molecules in the solution to the surface causes height increase in the transparent oxide film which in turn changes the optical path length difference (OPD). The intensity of the reflected light at a given wavelength is determined by the OPD between the top of the biomass layer and the Si/SiO_2 interface. The thicker the biomass layer gets, the higher the OPD becomes, and this increase in the OPD leads to a shift in the spectral reflectivity curve (Figure 14a) as well as change in the reflected light intensity at a specific wavelength. In IRIS optical setup, four LEDs with different wavelengths (455, 518, 598, and 635 nm) illuminate the substrate sequentially and the intensity of the reflected light is recorded by a CCD to generate an intensity image of the chip surface. Then, each pixel in this intensity image is fitted to the reflection function from which the thickness of the transparent film (oxide layer plus any biomass layer) is obtained. The calculated thickness difference for a given spot between two time points (before and after analyte incubation) is converted to biomass density by using simple conversion factors and an average mass density is calculated from replicate spots [84].

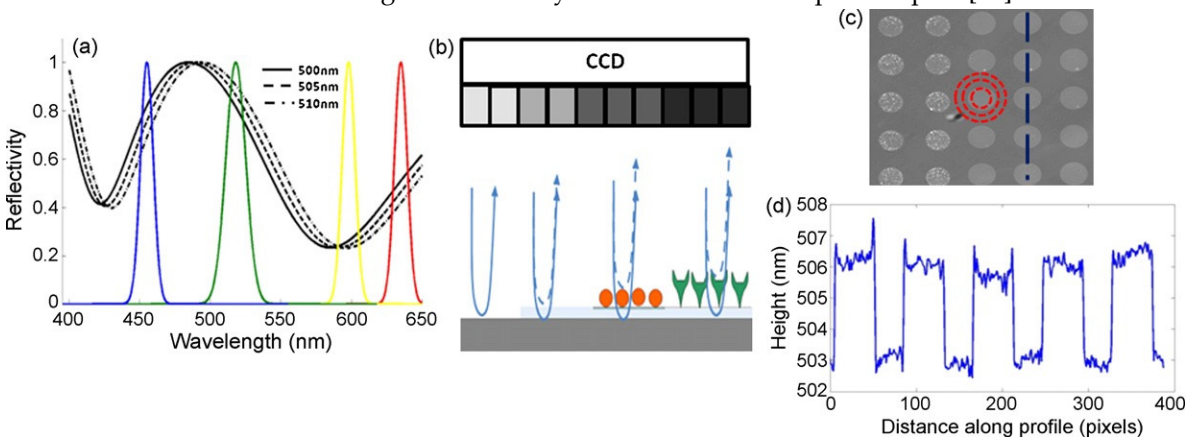

Preprints (www.preprints.org) | NOT PEER-REVIEWED | Posted: 27 April 2023 doi:10.20944/preprints202304.1013.v1

Figure 14. Principle of detection for IRIS: (a) shows the shift of the reflectivity curve due to 5 nm step increases in biofilm thickness on the chip surface. The reflectivity curve is sampled by using 4 different wavelength LEDs shown by the colored Gaussians. (b) Schematic of the sensor's imaging path illustrating biomass accumulation and associated grayscale intensity changes on the CCD camera. (c) Example of the sensor's surface with an array of protein spots. (d) Surface height profile along the blue dashed line in (c) across spots. Reproduced with permission from [82].

IRIS has been shown to be a versatile platform for monitoring protein-protein [85,86], DNA-DNA [87], and DNA-protein interactions [88], with applications into cytokine detection, identification of single nucleotide polymorphisms (SNPs), study of DNA binding proteins such as transcription factors, and antibody affinity measurements. IRIS was also used to detect intact vesicular stomatitis virus (VSV) particles with a detection limit close to 10^5 PFU/mL as well as internal viral proteins, such as nucleocapsid and matrix proteins by lysing the viruses with detergent [89]. IRIS platform was later modified to generate a digital detection modality to allow for the visualization and counting of single nanoparticles. This platform, referred to as single-particle IRIS (SP-IRIS), is composed of a single wavelength LED (525 nm) for illumination of the substrate, a high numerical aperture (NA = 0.8) objective to obtain a high spatial resolution image, and a CCD camera [90]. The thickness of the oxide layer was adjusted to optimize the interference of the particle scattered field with the reference field. The schematic of the optical setup for SP-IRIS is shown in Figure 15a.

For detecting biological nanoparticles such as viruses, an array of high affinity capture probes is generated on the surface that can selectively bind to the target virus. Capture probe immobilization is achieved by using a 3-D copolymer coating that provides NHS groups for the covalent attachment of amine-containing biomolecules [91]. When virus particles bind to the capture antibodies, scattered light from the particles interferes with the reference field reflecting from the Si/SiO_2 interface, which enhances the signal detected on the CCD camera. Particles captured on the chip surface show as bright dots in the recorded image (Figure 15b). SP-IRIS takes images of the spots in a microarray, and then these spot images are analyzed using custom software that finds particle-associated intensity peaks that correlate with a Gaussian profile. A forward model is applied to associate background normalized intensities (contrast) of the particles to particle size [90]. Therefore, for a given spot, the diffraction-limited dots with expected size range are selected using a Gaussian filter (red circles in Fig. 15b) and counted to obtain the number of virus particles bound to the spot. Pre-incubation particle count is subtracted from post-incubation particle count and the net virus count is divided by the spot area to obtain the bound virus density (number of particles per mm^2). Single particle detection ability of SP-IRIS offers a great advantage over ensemble-based methods, such as BLI, where many binding events need to occur to record a signal above the background noise. The high sensitivity achieved by single virus counting, when combined with the on-chip multiplexing ability, renders SP-IRIS an attractive platform for virus diagnostics applications.

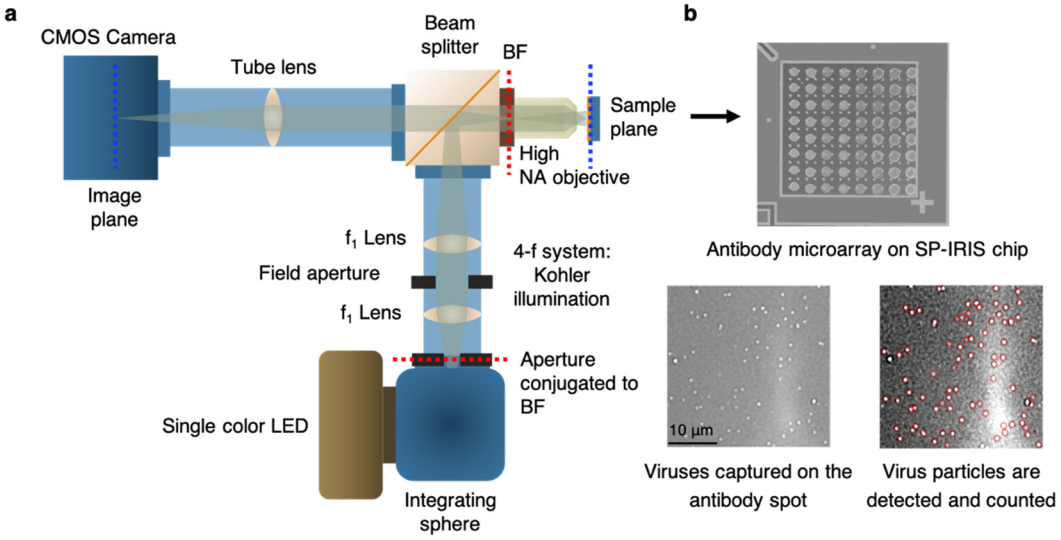

Preprints (www.preprints.org) | NOT PEER-REVIEWED | Posted: 27 April 2023 doi:10.20944/preprints202304.1013.v1

Figure 15. Optical setup of SP-IRIS and its application to virus detection. (a) Illustration of optical setup of SP-IRIS platform (BF: Back focal plane) (b) Top part is an example of SP-IRIS microarray chip with antibody spots. The image was taken with low-magnification modality of IRIS system. Each antibody spot is about 150 μm in diameter. Bottom images are zoomed in antibody spots from an SP-IRIS image after incubation with the specific virus sample. Captured virus particles appear as white dots, and they are detected (red circles) and counted using custom software. Reproduced with permission from [92].

2.7. Virus diagnostics applications of SP-IRIS

SP-IRIS can individually count and size the nanoparticles bound to capture probes on the sensor surface over a large sensor area, orders of magnitude larger than other virus imaging techniques such as electron microscopy. It allows for a large range of nanoparticle detection including both natural nanoparticles (e.g. viruses) and synthetic nanoparticles (e.g. gold nanospheres, gold nanorods) in a highly-multiplexed microarray format. So far, SP-IRIS has been shown to detect many different biological targets such as viruses [93], allergen-specific antibodies [94], extracellular vesicles [95], bacteria [96], and microRNA [97]. When the target is a nanoparticle itself, such as viruses, the detection can be done directly without using any secondary labels. If the biomolecule being searched for is below the size limit of the SP-IRIS (~ 30 nm), the target binding can be monitored by using specific detection probes attached to nanoparticle barcodes such as gold nanoparticles. Since this review's main topic is optical virus detection techniques, in this section, we will review the SP-IRIS studies demonstrating this application.

The work by Daaboul et al. was the first report to show SP-IRIS as a virus detection platform by demonstrating detection and sizing of individual H1N1 viruses [90]. In this work, H1N1 virus was immobilized on the sensor surface and imaged using both SP-IRIS and scanning electron microscopy (SEM) for the exact same field of view. Their results showed a one-to-one correspondence between SP-IRIS and SEM images confirming the particles observed in the SP-IRIS system are indeed virus particles, proving the sensor's ability to detect individual viruses (Figure 16). In the same work, by using the forward model mentioned before, they measured the mean size of the H1N1 particles as 116 nm with a size distribution of 17 nm, which is in good agreement with the reported H1N1virus size in the literature.

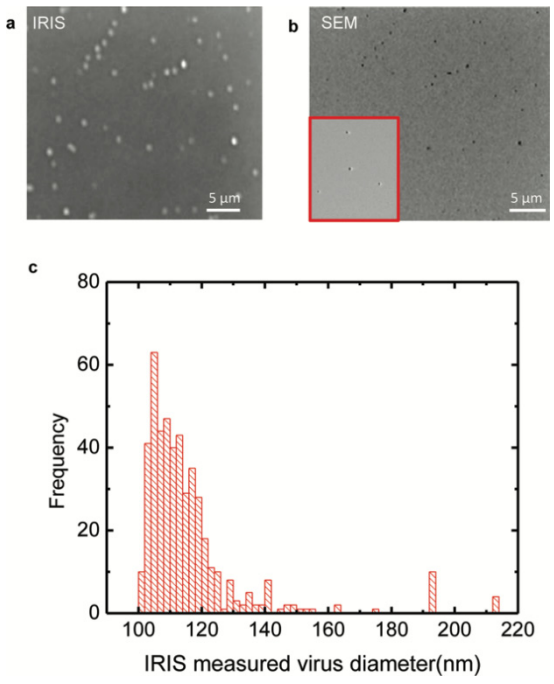

Figure 16. H1N1 virus detection and sizing: (a) SP-IRIS image of immobilized virus on the surface with the same field of view as the SEM image; (b) SEM image of immobilized virus on the surface; (c)

Preprints (www.preprints.org) | NOT PEER-REVIEWED | Posted: 27 April 2023 doi:10.20944/preprints202304.1013.v1

measured size distribution of immobilized virus using SP-IRIS. The mean size of the H1N1 was measured to be 116 ± 17 nm. Reproduced with permission from [90].

Following the first virus detection demonstration with immobilized H1N1 virus, SP-IRIS was shown to perform sensitive and multiplexed detection of whole viruses from serum and blood samples [93]. For this work, Daaboul et al. used genetically engineered vesicular stomatitis virus (VSV) pseudotypes that express surface glycoproteins of Ebola and Marburg viruses (rVSV-EBOV and rVSV-MARV) (Figure 17). They first arrayed EBOV and MARV specific antibodies on SP-IRIS chips and incubated the chips with either increasing concentrations of rVSV-EBOV only or the same increasing rVSV-EBOV concentrations in the presence of a constant concentration of rVSV-MARV. The virus solutions were prepared in serum containing 10^6 CFU/mL *E.coli* K12 to mimic a complex solution environment. Their results showed specific detection of rVSV-EBOV with increasing virus particles on anti-EBOV spots whereas anti-MARV spots had a constant signal in dual virus samples. The limit of detection (LOD) reported for rVSV-EBOV detection from serum and blood was 5×10^3 PFU/mL. A similar level of sensitivity was also reached for rVSV-MARV detection in the same study. This work demonstrated that SP-IRIS has a great potential to be used as a virus diagnostic technique with its ability of direct detection of the target viruses from complex samples without labeling and complicated sample preparation.

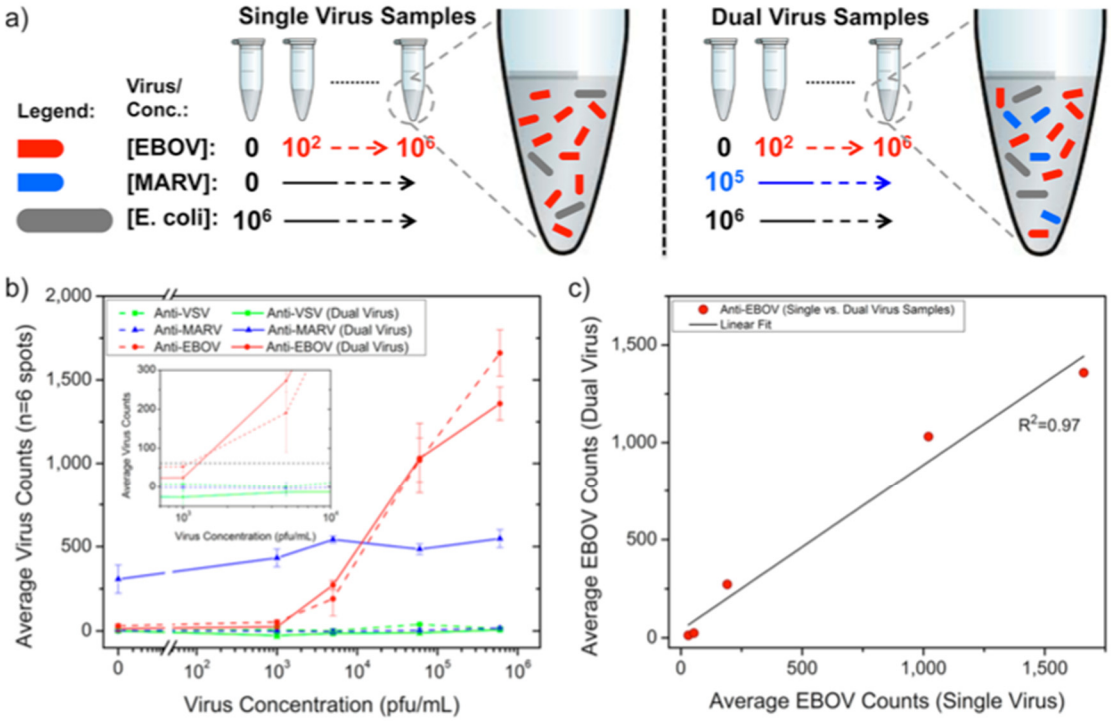

Figure 17. Duplexed detection of Ebola and Marburg-pseudotyped VSVs in serum and bacteria-containing samples. (a) Schematic of virus sample preparation. Both single and dual virus samples were prepared in serum containing 10^6 CFU/mL *E. coli* K12. (b) Anti-EBOV antibody spots showed an exponential response as the rVSV-EBOV concentration increased. Single and dual virus samples generated nearly identical virus counts on anti-EBOV spots for the same rVSV-EBOV titers, whereas, addition of Marburg pseudotype at a constant concentration gave a steady signal on anti-MARV antibody spots for all rVSV-EBOV concentrations. The inset displays an expanded view of virus concentrations around 10^3 PFU/mL; the dashed line represents the detection threshold calculated from the mean plus three standard deviations for the anti-EBOV spots incubated in the FBS alone. For (b) the lines connecting the data points are given only to guide the reader's eye between single and dual virus sample responses. (c) The response observed between the anti-EBOV spots in single and dual virus samples was similar as shown by the linear regression fit to a scatter plot of single virus sample type against the dual-sample. Reproduced with permission from [93].

Preprints (www.preprints.org) | NOT PEER-REVIEWED | Posted: 27 April 2023 doi:10.20944/preprints202304.1013.v1

SP-IRIS was further advanced to implement the ability of visualizing virus particles in-liquid environment, rendering the system a real-time imaging platform and eliminating washing and drying steps (Figure 18). In order to increase the contrast of the virus particles in liquid, some changes to the optical setup have been made such as use of a 40×, 0.9 NA objective and adjustment of the oxide thickness of the sensor chip. In this setup, the SP-IRIS chip is mounted in a disposable active microfluidic cartridge via a pressure-sensitive adhesive and the cartridge is fixed on the SP-IRIS stage. Scherr et al. reported a 50-fold increase in sensitivity compared to in-air measurements, leading to an LOD of 100 PFU/mL, for the detection of rVSV-EBOV from serum samples [98].

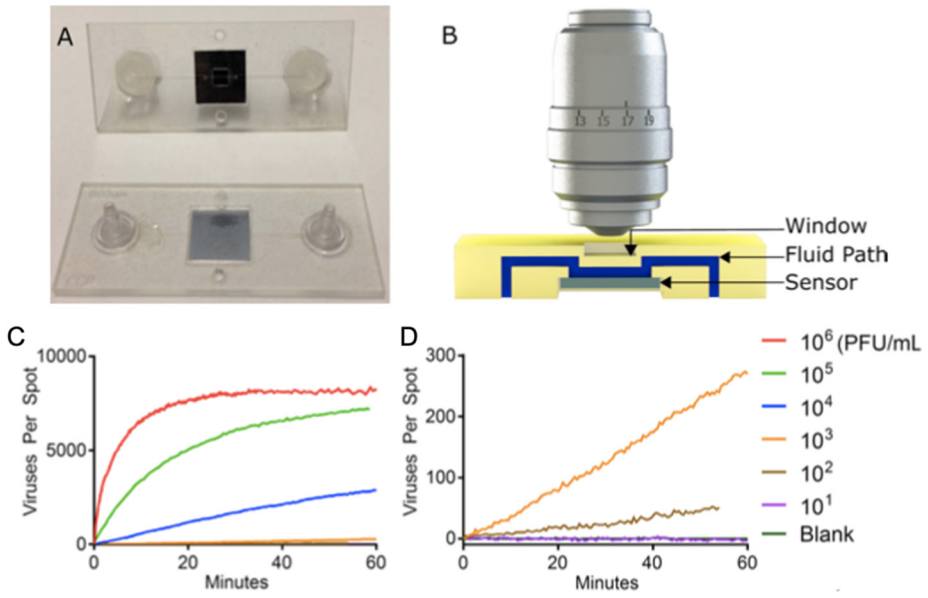

Figure 18. (A) Picture of the first-generation polymeric cartridge used for real-time virus imaging. (B) Cross section model which demonstrates the fluidic path (in blue), the sensor (in gray), and window (in yellow). Image is not to scale. (C) Accumulation of viruses being imaged on the sensor for a serial dilution ranging from 1 × 10^6 PFU/mL down to a blank sample. The high concentration samples show a very rapid accumulation of viruses followed by a saturation of the sensors. (D) Lower concentrations expanded, showing a linear accumulation of viruses and a limit of detection of 100 PFU/mL in less than 60 min. Reproduced with permission from [98].

To demonstrate the applicability of SP-IRIS to point-of-care diagnostics as a rapid detection method, a disposable passive microfluidic cartridge was designed with a multilayer polymer laminate structure and an integrated absorbent paper to establish capillary flow of the sample in the cartridge. This passive-flow integrated SP-IRIS achieved a better sensitivity than ELISA and a commercial rapid antigen test by detecting 10^4 PFU/mL rVSV-EBOV in less than 20 min [99,100]. A different study by Daaboul et al, demonstrated the usability of SP-IRIS for detection and characterization of a variety of virus sizes ranging from 40 nm for Zika virus to 360 nm for Vaccinia virus as well as filamentous virus particles like Ebola virus [101]. In addition, recently, Yurdakul et al. showed a different modality of SP-IRIS, referred to as single-particle interferometric microscopy, for obtaining shape and size information which will enable in depth morphological studies of viruses [102]. Collectively, these studies demonstrated the potential of SP-IRIS as a sensitive, fast, and multiplexed virus detection platform in a label-free and sample-to-answer format.

Besides the microfluidics integration and improvements in the optical setup of SP-IRIS, sensor chip surface chemistry has also been studied in an effort to increase the sensitivity of detection. By using a technique called DNA-directed antibody immobilization (DDI), Seymour et al. showed that capture antibodies can be elevated over the surface (~ 14 nm) through the use of DNA linkers attached to the antibodies [103]. This new surface preparation technique was shown to provide a 16-fold increase in sensitivity for rVSV-EBOV detection for a 15-min incubation period. This improvement is most likely due to the increased accessibility of the antibodies for virus binding as well as increased

Preprints (www.preprints.org) | NOT PEER-REVIEWED | Posted: 27 April 2023 doi:10.20944/preprints202304.1013.v1

functionality due to less surface attachment points in the antibody structure. This work was recently extended to a novel approach of mixing DNA-antibody conjugates and the virus sample in the solution phase before incubating the chip (Figure 19). This homogeneous method achieved a slightly better sensitivity than conventional DDI while decreasing the assay time [100]. Other advantages offered by this approach includes configurable sensor surface, decreased antibody amount needed for the assay, and long shelf-life of dried DNA-Ab conjugates.

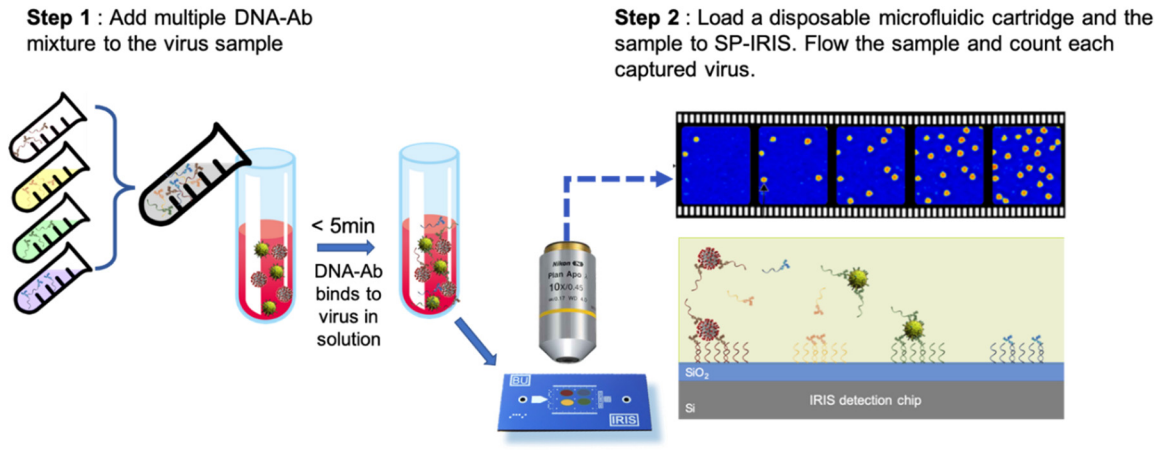

Figure 19. Schematic demonstration of the DNA-Ab conjugate-directed capture of the viruses on SP-IRIS. Step 1 involves mixing different DNA-conjugated antibodies, each targeting a different virus, and adding this mixture to the sample potentially containing a virus. After about a 5-min incubation, in Step 2, the sample is flowed over SP-IRIS chip that is assembled into a disposable microfluidic cartridge. Virus-DNA-Ab complexes are captured on the chip surface through DNA-DNA hybridization. Free DNA-Ab conjugates bound to the DNA spots are invisible in camera images. Only captured viruses appear as bright dots.

SP-IRIS offers significant advantages compared to the other optical biosensing platforms mentioned in this review. First of all, SP-IRIS has a comparable sensitivity to SPR, the most commonly used label-free biosensor, while having higher multiplexing capability, substantially less expensive substrates, and shorter analysis time [86]. Moreover, the detection principle of SP-IRIS is immune to bulk-effect, a major problem of SPR-based systems that is caused by the changes in the refractive index of the solution. SP-IRIS overcomes any background-related affect by imaging only the nanoparticles that are bound to the surface. Moreover, unlike optical resonator-based sensors, SP-IRIS signal is not affected by environmental factors such as temperature changes or binding position of the particles on the sensor. Thus, SP-IRIS combines robust and reliable signal transduction mechanism with high-sensitivity, high-throughput detection in a cost-effective and easy-to-use platform. All of these features make SP-IRIS a perfect candidate for virus diagnostics applications especially for POC applications.

3. Conclusions

In this review, we discussed several surface-based optical biosensing techniques that have been used to detect and characterize viruses. Recent outbreaks revealed the importance of development of virus diagnostic platforms that are sensitive, reliable, rapid and affordable. Multiplexing ability is also considered critical especially in cases where the diseases with similar physical symptoms occur at the same time such as COVID-19 and flu. In addition, the ideal virus detection platform should operate with minimum sample preparation in a preferably enclosed environment.

The biggest advantage of SP-IRIS compared to other optical techniques lies in its ability to detect single viruses in a robust and cost-efficient platform. Moreover, recent advancements in SP-IRIS enabled it to work with integrated microfluidic cartridges, eliminating chip handling steps. SP-IRIS can also perform sensitive and specific detection from complex media such as blood and serum,

decreasing the assay time and complexity. In addition, lately, data processing for SP-IRIS assays was improved such that it can be done in real-time. Therefore, the assay results are available at the end of the incubation period which is less than 30 min. All these developments have brought SP-IRIS closer to realizing the concept of ideal virus diagnostic platform that is attractive for both in-clinic and field use.

Acknowledgments: Authors would like to thank John H. Connor (Boston University), Marcella Chiari and Marina Cretich (CNR, Milan), and past and current members of Ünlü lab at Boston University for their contributions to the IRIS and SP-IRIS work presented in this review.

References

1. C.-19 M. J. H. C. R. Center, "No Title," *https://coronavirus.jhu.edu/map.html*. .
2. D. Raoult, N. Mouffok, I. Bitam, R. Piarroux, and M. Drancourt, "Plague: History and contemporary analysis," *J. Infect.*, vol. 66, no. 1, pp. 18–26, 2013.
3. J. B. Harris, R. C. LaRocque, F. Qadri, E. T. Ryan, and S. B. Calderwood, "Cholera," in *The Lancet*, 2012, vol. 379, no. 9835, pp. 2466–2476.
4. P. R. Saunders-Hastings and D. Krewski, "Reviewing the history of pandemic influenza: Understanding patterns of emergence and transmission," *Pathogens*, vol. 5, no. 4. 2016.
5. P. M. Sharp and B. H. Hahn, "Origins of HIV and the AIDS pandemic.," *Cold Spring Harb. Perspect. Med.*, vol. 1, no. 1, p. a006841, Sep. 2011.
6. N. P. A. S. Johnson and J. Mueller, "Updating the accounts: global mortality of the 1918-1920 'Spanish' influenza pandemic.," *Bull. Hist. Med.*, vol. 76, no. 1, pp. 105–115, 2002.
7. K. J. HENRICKSON, "Advances in the laboratory diagnosis of viral respiratory disease," *Pediatr. Infect. Dis. J.*, vol. 23, no. 1, 2004.
8. C. S. Goldsmith and S. E. Miller, "Modern uses of electron microscopy for detection of viruses.," *Clin. Microbiol. Rev.*, vol. 22, no. 4, pp. 552–563, Oct. 2009.
9. H. Hopfer *et al.*, "Hunting coronavirus by transmission electron microscopy - a guide to SARS-CoV-2-associated ultrastructural pathology in COVID-19 tissues.," *Histopathology*, vol. 78, no. 3, pp. 358–370, Feb. 2021.
10. N. Bhalla, P. Jolly, N. Formisano, and P. Estrela, "Introduction to biosensors.," *Essays Biochem.*, vol. 60, no. 1, pp. 1–8, Jun. 2016.
11. X. Fan, I. M. White, S. I. Shopova, H. Zhu, J. D. Suter, and Y. Sun, "Sensitive optical biosensors for unlabeled targets: A review," *Anal. Chim. Acta*, vol. 620, no. 1–2, pp. 8–26, 2008.
12. P. Damborský, J. Švitel, and J. Katrlík, "Optical biosensors," *Essays Biochem.*, vol. 60, no. 1, pp. 91–100, 2016.
13. J.-F. Masson, "Surface Plasmon Resonance Clinical Biosensors for Medical Diagnostics," *ACS Sensors*, vol. 2, no. 1, pp. 16–30, Jan. 2017.
14. A. K. Singh, S. Mittal, M. Das, A. Saharia, and M. Tiwari, "Optical biosensors: a decade in review," *Alexandria Eng. J.*, vol. 67, pp. 673–691, 2023.
15. M. S. Hejazi, M. H. Pournaghi-Azar, and F. Ahour, "Electrochemical detection of short sequences of hepatitis C 3a virus using a peptide nucleic acid-assembled gold electrode," *Anal. Biochem.*, vol. 399, no. 1, pp. 118–124, 2010.
16. M. H. Pournaghi-Azar, F. Ahour, and M. S. Hejazi, "Direct detection and discrimination of double-stranded oligonucleotide corresponding to hepatitis C virus genotype 3a using an electrochemical DNA biosensor based on peptide nucleic acid and double-stranded DNA hybridization.," *Anal. Bioanal. Chem.*, vol. 397, no. 8, pp. 3581–3587, Aug. 2010.
17. S. Zheng, D.-K. Kim, T. J. Park, S. J. Lee, and S. Y. Lee, "Label-free optical diagnosis of hepatitis B virus with genetically engineered fusion proteins," *Talanta*, vol. 82, no. 2, pp. 803–809, 2010.
18. B. D. Gupta, A. M. Shrivastav, and S. P. Usha, "Surface Plasmon Resonance-Based Fiber Optic Sensors Utilizing Molecular Imprinting," *Sensors*, vol. 16, no. 9, 2016.
19. S. B. Nanjunda *et al.*, "Emerging nanophotonic biosensor technologies for virus detection," *Nanophotonics*, vol. 11, no. 22, pp. 5041–5059, 2022.
20. P. Mehrotra, "Biosensors and their applications – A review," *J. Oral Biol. Craniofacial Res.*, vol. 6, no. 2, pp. 153–159, 2016.
21. T. Celiker *et al.*, "Fluorescent bioassay for SARS-CoV-2 detection using polypyrene-g-poly(ε-caprolactone) prepared by simultaneous photoinduced step-growth and ring-opening polymerizations," *Microchim. Acta*, vol. 189, no. 5, 2022.
22. A. Sharma *et al.*, "Optical biosensors for diagnostics of infectious viral disease: A recent update," *Diagnostics*, vol. 11, no. 11, 2021.
23. F. Kulzer and M. Orrit, "SINGLE-MOLECULE OPTICS," *Annu. Rev. Phys. Chem.*, vol. 55, no. 1, pp. 585–611, Jun. 2004.

24. M. Shirani, H. Kalantari, M. J. Khodayar, M. Kouchak, and N. Rahbar, "A novel strategy for detection of small molecules based on aptamer/gold nanoparticles/graphitic carbon nitride nanosheets as fluorescent biosensor.," *Talanta*, vol. 219, p. 121235, Nov. 2020.
25. A. M. Salama, G. Yasin, M. Zourob, and J. Lu, "Fluorescent Biosensors for the Detection of Viruses Using Graphene and Two-Dimensional Carbon Nanomaterials," *Biosensors*, vol. 12, no. 7, 2022.
26. R. M. Clegg, "Fluorescence resonance energy transfer.," *Curr. Opin. Biotechnol.*, vol. 6, no. 1, pp. 103–110, Feb. 1995.
27. H. Maddali, C. E. Miles, J. Kohn, and D. M. O'Carroll, "Optical Biosensors for Virus Detection: Prospects for SARS-CoV-2/COVID-19," *ChemBioChem*, vol. 22, no. 7, pp. 1176–1189, 2021.
28. A. Sharma *et al.*, "Designed Strategies for Fluorescence-Based Biosensors for the Detection of Mycotoxins," *Toxins (Basel).*, vol. 10, no. 5, 2018.
29. F. Ekiz-Kanik, D. D. Sevenler, N. L. Ünlü, M. Chiari, and M. S. Ünlü, "Surface chemistry and morphology in single particle optical imaging," *Nanophotonics*, vol. 6, no. 4. pp. 713–730, 2017.
30. D. Jiang, Y. Tian, Y. Zhang, X. Lu, D. Xiao, and C. Zhou, "One-step fast and label-free imaging array for multiplexed detection of trace avian influenza viruses," *Anal. Chim. Acta*, vol. 1171, p. 338645, 2021.
31. C. Hepp *et al.*, "Viral detection and identification in 20 min by rapid single-particle fluorescence in-situ hybridization of viral RNA," *Sci. Rep.*, vol. 11, no. 1, pp. 1–12, 2021.
32. N. Shiaelis *et al.*, "Virus Detection and Identification in Minutes Using Single-Particle Imaging and Deep Learning," *ACS Nano*, vol. 17, no. 1, pp. 697–710, 2023.
33. S. J. Yeo *et al.*, "Smartphone-based fluorescent diagnostic system for highly pathogenic H5N1 viruses," *Theranostics*, vol. 6, no. 2, pp. 231–242, 2016.
34. S. Xu *et al.*, "Highly Uniform Gold Nanobipyramids for Ultrasensitive Colorimetric Detection of Influenza Virus.," *Anal. Chem.*, vol. 89, no. 3, pp. 1617–1623, Feb. 2017.
35. Y. Choi, J. H. Hwang, and S. Y. Lee, "Recent Trends in Nanomaterials-Based Colorimetric Detection of Pathogenic Bacteria and Viruses.," *Small methods*, vol. 2, no. 4, p. 1700351, Apr. 2018.
36. Y. Wu, J. Feng, G. Hu, E. Zhang, and H.-H. Yu, "Colorimetric Sensors for Chemical and Biological Sensing Applications," *Sensors*, vol. 23, no. 5, 2023.
37. T. Yoneyama *et al.*, "Rapid and real-time detection of hepatitis A virus by reverse transcription loop-mediated isothermal amplification assay," *J. Virol. Methods*, vol. 145, no. 2, pp. 162–168, 2007.
38. I. M. Khoris, A. D. Chowdhury, T.-C. Li, T. Suzuki, and E. Y. Park, "Advancement of capture immunoassay for real-time monitoring of hepatitis E virus-infected monkey.," *Anal. Chim. Acta*, vol. 1110, pp. 64–71, May 2020.
39. C. N. Loynachan *et al.*, "Platinum Nanocatalyst Amplification: Redefining the Gold Standard for Lateral Flow Immunoassays with Ultrabroad Dynamic Range.," *ACS Nano*, vol. 12, no. 1, pp. 279–288, Jan. 2018.
40. R. Wang *et al.*, "Rapid Diagnostic Platform for Colorimetric Differential Detection of Dengue and Chikungunya Viral Infections," *Anal. Chem.*, vol. 91, no. 8, pp. 5415–5423, Apr. 2019.
41. Y. W. Fen, W. M. M. Yunus, N. A. Yusof, N. S. Ishak, N. A. S. Omar, and A. A. Zainudin, "Preparation, characterization and optical properties of ionophore doped chitosan biopolymer thin film and its potential application for sensing metal ion," *Optik (Stuttg).*, vol. 126, no. 23, pp. 4688–4692, 2015.
42. A. A. Zainudin, Y. W. Fen, N. A. Yusof, and N. A. S. Omar, "Structural, optical and sensing properties of ionophore doped graphene based bionanocomposite thin film," *Optik (Stuttg).*, vol. 144, pp. 308–315, 2017.
43. N. A. S. Omar and Y. W. Fen, "Recent development of SPR spectroscopy as potential method for diagnosis of dengue virus E-protein," *Sens. Rev.*, vol. 38, no. 1, pp. 106–116, Jan. 2018.
44. S. Murali, R. R. Rustandi, X. Zheng, A. Payne, and L. Shang, "Applications of Surface Plasmon Resonance and Biolayer Interferometry for Virus-Ligand Binding.," *Viruses*, vol. 14, no. 4, Mar. 2022.
45. A. Rasooly and K. E. Herold, "Biosensors and biodetection: methods and protocols. Preface.," *Methods in molecular biology (Clifton, N.J.)*, vol. 503. United States, pp. v–ix, 2009.
46. R. L. Caygill, G. E. Blair, and P. A. Millner, "A review on viral biosensors to detect human pathogens.," *Anal. Chim. Acta*, vol. 681, no. 1–2, pp. 8–15, Nov. 2010.
47. X. Zheng, C. Bi, Z. Li, M. Podariu, and D. S. Hage, "Analytical methods for kinetic studies of biological interactions: A review.," *J. Pharm. Biomed. Anal.*, vol. 113, pp. 163–180, Sep. 2015.
48. M. M. Hassan, F. S. Sium, F. Islam, and S. M. Choudhury, "A review on plasmonic and metamaterial based biosensing platforms for virus detection," *Sens. Bio-Sensing Res.*, vol. 33, p. 100429, 2021.
49. P. S. Pandey, S. K. Raghuwanshi, A. Shadab, M. T. I. Ansari, U. K. Tiwari, and S. Kumar, "SPR Based Biosensing Chip for COVID-19 Diagnosis-A Review.," *IEEE Sens. J.*, vol. 22, no. 14, pp. 13800–13810, Jul. 2022.
50. Y.-F. Chang *et al.*, "Simple Strategy for Rapid and Sensitive Detection of Avian Influenza A H7N9 Virus Based on Intensity-Modulated SPR Biosensor and New Generated Antibody.," *Anal. Chem.*, vol. 90, no. 3, pp. 1861–1869, Feb. 2018.
51. H. Yoo, J. Shin, J. Sim, H. Cho, and S. Hong, "Reusable surface plasmon resonance biosensor chip for the detection of H1N1 influenza virus," *Biosens. Bioelectron.*, vol. 168, p. 112561, 2020.

52. E. Mauriz, "Recent Progress in Plasmonic Biosensing Schemes for Virus Detection.," *Sensors (Basel).*, vol. 20, no. 17, Aug. 2020.
53. A. M. Shrivastav, U. Cvelbar, and I. Abdulhalim, "A comprehensive review on plasmonic-based biosensors used in viral diagnostics," *Commun. Biol.*, vol. 4, no. 1, pp. 1–12, 2021.
54. M. Puiu and C. Bala, "SPR and SPR Imaging: Recent Trends in Developing Nanodevices for Detection and Real-Time Monitoring of Biomolecular Events.," *Sensors (Basel).*, vol. 16, no. 6, Jun. 2016.
55. A. V Kabashin *et al.*, "Plasmonic nanorod metamaterials for biosensing.," *Nat. Mater.*, vol. 8, no. 11, pp. 867–871, Nov. 2009.
56. M. Couture, S. S. Zhao, and J.-F. Masson, "Modern surface plasmon resonance for bioanalytics and biophysics," *Phys. Chem. Chem. Phys.*, vol. 15, no. 27, pp. 11190–11216, 2013.
57. L. Guo, J. A. Jackman, H.-H. Yang, P. Chen, N.-J. Cho, and D.-H. Kim, "Strategies for enhancing the sensitivity of plasmonic nanosensors," *Nano Today*, vol. 10, no. 2, pp. 213–239, 2015.
58. J. Kim *et al.*, "Heteroassembled gold nanoparticles with sandwich-immunoassay LSPR chip format for rapid and sensitive detection of hepatitis B virus surface antigen (HBsAg).," *Biosens. Bioelectron.*, vol. 107, pp. 118–122, Jun. 2018.
59. S. Kim, S. Lee, and H. J. Lee, "An aptamer-aptamer sandwich assay with nanorod-enhanced surface plasmon resonance for attomolar concentration of norovirus capsid protein," *Sensors Actuators B Chem.*, vol. 273, pp. 1029–1036, 2018.
60. M. Li, S. K. Cushing, and N. Wu, "Plasmon-enhanced optical sensors: a review," *Analyst*, vol. 140, no. 2, pp. 386–406, 2015.
61. S. M. Mousavi *et al.*, "Highly Sensitive Flexible SERS-Based Sensing Platform for Detection of COVID-19.," *Biosensors*, vol. 12, no. 7, Jun. 2022.
62. O. Ambartsumyan, D. Gribanyov, V. Kukushkin, A. Kopylov, and E. Zavyalova, "SERS-Based Biosensors for Virus Determination with Oligonucleotides as Recognition Elements.," *Int. J. Mol. Sci.*, vol. 21, no. 9, May 2020.
63. F. Saviñon-Flores *et al.*, "A Review on SERS-Based Detection of Human Virus Infections: Influenza and Coronavirus," *Biosensors*, vol. 11, no. 3, 2021.
64. H. Liu *et al.*, "Development of a SERS-based lateral flow immunoassay for rapid and ultra-sensitive detection of anti-SARS-CoV-2 IgM/IgG in clinical samples.," *Sens. Actuators. B. Chem.*, vol. 329, p. 129196, Feb. 2021.
65. Z. Zhang *et al.*, "Rapid detection of viruses: Based on silver nanoparticles modified with bromine ions and acetonitrile," *Chem. Eng. J.*, vol. 438, p. 135589, 2022.
66. D. K. Armani, T. J. Kippenberg, S. M. Spillane, and K. J. Vahala, "Ultra-high-Q toroid microcavity on a chip," *Nature*, vol. 421, no. 6926, pp. 925–928, 2003.
67. M. Iqbal *et al.*, "Label-free biosensor arrays based on silicon ring resonators and high-speed optical scanning instrumentation," *IEEE J. Sel. Top. Quantum Electron.*, vol. 16, no. 3, pp. 654–661, 2010.
68. M. Baaske and F. Vollmer, "Optical resonator biosensors: Molecular diagnostic and nanoparticle detection on an integrated platform," *ChemPhysChem*, vol. 13, no. 2, pp. 427–436, 2012.
69. H. Ahmadi *et al.*, "Evaluation of single virus detection through optical biosensor based on microsphere resonator," *Optik (Stuttg).*, vol. 125, no. 14, pp. 3599–3602, 2014.
70. F. Vollmer, S. Arnold, and D. Keng, "Single virus detection from the reactive shift of a whispering-gallery mode.," *Proc. Natl. Acad. Sci. U. S. A.*, vol. 105, no. 52, pp. 20701–20704, Dec. 2008.
71. J. Zhu, Ş. K. Özdemir, L. He, D.-R. Chen, and L. Yang, "Single virus and nanoparticle size spectrometry by whispering-gallery-mode microcavities," *Opt. Express*, vol. 19, no. 17, p. 16195, Aug. 2011.
72. L. He, Ş. K. Özdemir, J. Zhu, W. Kim, and L. Yang, "Detecting single viruses and nanoparticles using whispering gallery microlasers," *Nat. Nanotechnol.*, vol. 6, no. 7, pp. 428–432, 2011.
73. P. Steglich, M. Hülsemann, B. Dietzel, and A. Mai, "Optical Biosensors Based on Silicon-On-Insulator Ring Resonators: A Review.," *Molecules*, vol. 24, no. 3, Jan. 2019.
74. W. Bogaerts *et al.*, "Silicon microring resonators," *Laser Photonics Rev.*, vol. 6, no. 1, pp. 47–73, 2012.
75. A. J. Qavi *et al.*, "Rapid detection of an Ebola biomarker with optical microring resonators.," *Cell reports methods*, vol. 2, no. 6, p. 100234, Jun. 2022.
76. B. Koo *et al.*, "An isothermal, label-free, and rapid one-step RNA amplification/detection assay for diagnosis of respiratory viral infections," *Biosens. Bioelectron.*, vol. 90, no. November 2016, pp. 187–194, 2017.
77. G. G. Daaboul, C. A. Lopez, A. Yurt, B. B. Goldberg, J. H. Connor, and M. S. Ünlü, "Label-free optical biosensors for virus detection and characterization," *IEEE J. Sel. Top. Quantum Electron.*, vol. 18, no. 4, pp. 1422–1433, 2012.
78. V. Kamat and A. Rafique, "Designing binding kinetic assay on the bio-layer interferometry (BLI) biosensor to characterize antibody-antigen interactions.," *Anal. Biochem.*, vol. 536, pp. 16–31, Nov. 2017.
79. J. V Dzimianski, N. Lorig-Roach, S. M. O'Rourke, D. L. Alexander, J. M. Kimmey, and R. M. DuBois, "Rapid and sensitive detection of SARS-CoV-2 antibodies by biolayer interferometry," *Sci. Rep.*, vol. 10, no. 1, p. 21738, 2020.

80. A. Yurt, G. G. Daaboul, J. H. Connor, B. B. Goldberg, and M. Selim Ünlü, "Single nanoparticle detectors for biological applications," *Nanoscale*, vol. 4, no. 3, pp. 715–726, Feb. 2012.
81. A. Mitra, F. Ignatovich, and L. Novotny, "Real-time optical detection of single human and bacterial viruses based on dark-field interferometry.," *Biosens. Bioelectron.*, vol. 31, no. 1, pp. 499–504, Jan. 2012.
82. G. G. Daaboul *et al.*, "LED-based Interferometric Reflectance Imaging Sensor for quantitative dynamic monitoring of biomolecular interactions," *Biosens. Bioelectron.*, vol. 26, no. 5, pp. 2221–2227, 2011.
83. E. Özkumur *et al.*, "Label-free and dynamic detection of biomolecular interactions for high-throughput microarray applications.," *Proc. Natl. Acad. Sci. U. S. A.*, vol. 105, no. 23, pp. 7988–7992, Jun. 2008.
84. E. Özkumur *et al.*, "Quantification of DNA and protein adsorption by optical phase shift," *Biosens. Bioelectron.*, 2009.
85. S. Ahn, D. S. Freedman, P. Massari, M. Cabodi, and M. S. Ünlü, "A Mass-Tagging Approach for Enhanced Sensitivity of Dynamic Cytokine Detection Using a Label-Free Biosensor," *Langmuir*, vol. 29, no. 17, pp. 5369–5376, Apr. 2013.
86. A. M. Marn, J. Needham, E. Chiodi, and M. S. Ünlü, "Multiplexed, high-sensitivity measurements of antibody affinity using interferometric reflectance imaging sensor," *Biosensors*, vol. 11, no. 12, pp. 1–9, 2021.
87. E. Özkumur *et al.*, "Label-free microarray imaging for direct detection of DNA hybridization and single-nucleotide mismatches," *Biosens. Bioelectron.*, vol. 25, no. 7, pp. 1789–1795, Mar. 2010.
88. S. Ahn *et al.*, "TATA binding proteins can recognize nontraditional DNA sequences.," *Biophys. J.*, vol. 103, no. 7, pp. 1510–1517, Oct. 2012.
89. C. A. Lopez *et al.*, "Label-free multiplexed virus detection using spectral reflectance imaging," *Biosens. Bioelectron.*, vol. 26, no. 8, pp. 3432–3437, 2011.
90. G. G. Daaboul, A. Yurt, X. Zhang, G. M. Hwang, B. B. Goldberg, and M. S. Ünlü, "High-throughput detection and sizing of individual low-index nanoparticles and viruses for pathogen identification," *Nano Lett.*, vol. 10, no. 11, pp. 4727–4731, 2010.
91. M. Cretich, G. Pirri, F. Damin, I. Solinas, and M. Chiari, "A new polymeric coating for protein microarrays," *Anal. Biochem.*, vol. 332, no. 1, pp. 67–74, 2004.
92. E. Seymour, M. S. Ünlü, and J. H. Connor, "A high-throughput single-particle imaging platform for antibody characterization and a novel competition assay for therapeutic antibodies.," *Sci. Rep.*, vol. 13, no. 1, p. 306, Jan. 2023.
93. G. G. Daaboul, C. A. Lopez, J. Chinnala, B. B. Goldberg, J. H. Connor, and M. Selim Ünlü, "Digital sensing and sizing of vesicular stomatitis virus pseudotypes in complex media: A model for ebola and marburg detection," *ACS Nano*, vol. 8, no. 6, pp. 6047–6055, 2014.
94. M. R. Monroe, G. G. Daaboul, A. Tuysuzoglu, C. A. Lopez, F. F. Little, and M. S. Ünlü, "Single nanoparticle detection for multiplexed protein diagnostics with attomolar sensitivity in serum and unprocessed whole blood," *Anal. Chem.*, vol. 85, no. 7, pp. 3698–3706, 2013.
95. G. G. Daaboul *et al.*, "Digital Detection of Exosomes by Interferometric Imaging," *Sci. Rep.*, vol. 6, no. 1, p. 37246, 2016.
96. N. Zaraee *et al.*, "Highly sensitive and label-free digital detection of whole cell E. coli with Interferometric Reflectance Imaging," *Biosens. Bioelectron.*, vol. 162, p. 112258, 2020.
97. F. Ekiz Kanik *et al.*, "Attomolar sensitivity microRNA detection using real-time digital microarrays," *Sci. Rep.*, vol. 12, no. 1, p. 16220, 2022.
98. S. M. Scherr *et al.*, "Real-Time Capture and Visualization of Individual Viruses in Complex Media," *ACS Nano*, vol. 10, no. 2, pp. 2827–2833, 2016.
99. S. M. Scherr *et al.*, "Disposable cartridge platform for rapid detection of viral hemorrhagic fever viruses," *Lab Chip*, vol. 17, no. 5, pp. 917–925, 2017.
100. E. Seymour, N. L. Ünlü, E. P. Carter, J. H. Connor, and M. S. Ünlü, "Configurable Digital Virus Counter on Robust Universal DNA Chips," *ACS Sensors*, vol. 6, no. 1, pp. 229–237, 2021.
101. G. G. Daaboul *et al.*, "Enhanced light microscopy visualization of virus particles from Zika virus to filamentous ebolaviruses," *PLoS One*, vol. 12, no. 6, pp. 1–15, 2017.
102. C. Yurdakul *et al.*, "High-Throughput, High-Resolution Interferometric Light Microscopy of Biological Nanoparticles," *ACS Nano*, vol. 14, no. 2, pp. 2002–2013, 2020.
103. E. Seymour *et al.*, "DNA-Directed Antibody Immobilization for Enhanced Detection of Single Viral Pathogens," *Anal. Chem.*, vol. 87, no. 20, pp. 10505–10512, 2015.